NASA CR-112334

AN INVESTIGATION OF THE COMPRESSIVE STRENGTH OF PRD-49-III/EPOXY COMPOSITES

by

Satish V. Kulkarni, Joseph S. Rice
and
B. Walter Rosen

Prepared under Contract No. NAS1-11780 by

Materials Sciences Corporation
Blue Bell Office Campus, Blue Bell, Pa. 19422

for

NATIONAL AERONAUTICS AND SPACE ADMINISTRATION

June 1973

FORWARD

This final report was prepared by the Materials Sciences Corporation under contract NAS1-11780 for the National Aeronautics and Space Administration. Mr. Donald J. Baker of the Langley Research Center was the Technical Representative. The assistance of Dr. John Moore, Dr. Donald Sturgeon and Mr. Gerald Severin of the Engineering Experimental Station of E. I. DuPont de Nemours Co., Inc., in the experimental phase of this program is gratefully acknowledged.

TABLE OF CONTENTS

LIST OF SYMBOLS

A_n	Constants;
$2c+h$	Fiber center to center distance;
E_m, E_f	Matrix and fiber elastic moduli, respectively;
f_n	Function of κ, n, h, E_f, ℓ and G_f;
g_1, g_2	Functions of G_m, G_f, h, c;
G_m, G_f	Matrix and fiber shear moduli, respectively;
G_{LT}	In-plane shear modulus of composite;
h	Fiber diameter or reinforcement thickness;
k	Fiber-matrix interface slippage parameter;
ℓ	Length of composite specimen;
n	Wave number;
ΔT	Change in potential energy;
u_x, u_y	Displacement in the x and y directions, respectively;
v_f	Fiber volume fraction;
ΔV_m, ΔV_f	Changes in the strain energy of the matrix and fiber, respectively;
x, y	Coordinate directions;
α_f	Shear strain in fiber due to τ_{xy};
γ_f	Bending shear strain in fiber;
γ	Shear strain;
κ	Shear coefficient;
ϕ_o	Initial misalignment of the fiber;
$\sigma_{c(E)}$	Critical composite stress for extensional mode;
$\sigma_{c(s)}$	Critical composite stress for shear mode;
σ_f	Fiber stress;
τ	Interlaminar shear strength or shear stress;
τ_{xy}	Shear stress.

I. INTRODUCTION *

Many unidirectional fiber composite materials having high axial tensile strengths have been developed. Most of these have also been found to have a high axial compressive strength. Although theories have been presented which attempt to explain the reason for this high compressive strength, the literature reflects an incomplete understanding of this behavior. However, the fact that many fiber composite materials demonstrate relatively equal and high tensile and compressive strengths makes them acceptable for a wide range of engineering applications.

In the case of PRD-49-III/epoxy composites, it has been found experimentally that compressive strengths are of the order of 40ksi (.275 GN/m^2), or only some 20% of the tensile strength of these unidirectional fiber composites. Although many structural designs can efficiently accomodate materials in which there is a wide disparity between tensile and compressive strengths, there remains the uncertainty associated with the lack of understanding of the reasons for this low compressive strength. The study conducted herein is to enhance the understanding of the compressive behavior of this material, and through this understanding to develop ways of improving the compressive strength. This study is a combined theoretical and experimental study of the compressive strength of PRD-49-III/epoxy composites.

Techniques for improving the compressive strength of PRD-49-III/epoxy composites were investigated experimentally and theoretically and the tasks outlined below were performed.

Initially, a test plan was formulated. The specimen configuration adequacy was determined by different compression test specimens using both E-Glass/epoxy and PRD-49-III/epoxy to define a baseline specimen configuration. Then tests were performed to evaluate the effect of a wide range of variables including matrix properties, interface properties, fiber prestressing, secondary reinforcement, and others on the ultimate compressive strength of PRD-49-III/epoxy composites.

Failure to obtain a substantial increase in the compressive strength prompted Scanning Electron Microscope studies. The photomicrographs thus obtained illustrated some unique fiber properties such as kink band formation and lack of good bond with matrix. These suggest possible reasons for the low ultimate compressive stress.

---

* - The contract research effort which has lead to the results in this report was financially supported by USAAMRDL (Langley Directorate).

Finally, the theoretical study was performed to assess the influence of fiber anisotropy and lack of perfect bond between fiber and matrix on the shear mode microbuckling.

In spite of the fact that the theoretical analysis has quantitatively failed to predict and the experimental investigation to improve the compressive strength, it can be concluded that the present investigation has indeed enhanced the understanding of the compressive failure mechanism of PRD-49-III composites.

II. PROGRAM OVERVIEW

It is known that highly oriented polymers give attractive specific moduli. The first organic fiber produced with a moderately high modulus was DuPont's wholly aromatic nylon, Nomex. Recently, DuPont has introduced a new series of organic fibers coded PRD-49. These fibers are also available commercially since early 1972. PRD-49 fibers are high modulus, anisotropic, high tensile strength, high stability, premium organic fibers with the low density, low conductivity and textile processability normally associated with conventional organic fibers. Some of the pertinent properties of PRD-49-III fiber and unidirectional laminate are tabulated in Tables I and II. PRD-49-III has proven to be cost effective, weight reducing replacements for E-Glass in aircraft interior trim and exterior fairings, can compete with S-Glass in filament wound missile components and with Aluminum in aircraft skin. The low dielectric constant has led to evaluation in radome applications where needs for radar transparency, corrosion and impact resistance make Aluminum honeycomb unsuitable. A detailed summary of the properties and applications has been given by Moore [1], Sturgeon, et al [2] and Moore, et al [3].

The high specific modulus of PRD-49-III is associated with a highly oriented crystallized microstructure. While this type of microstructure is desirable for good tensile properties, it is detrimental insofar as the compressive strength is concerned. It has been suggested that a highly aligned crystalline microstructure (in metals or polymers) leads to a low compressive strength. This is because the structure buckles at low stresses and deformation bands appear. It is also important to note in this context that an increase in the modulus of graphite fibers results in a decrease in the compressive strength. However, for moderatly low modulus graphite fibers such as HTS, the documented value of tensile and compressive strengths are identical.

From the point of view of mechanics, it would appear that the apparent low compressive strength may be a result of such factors as fiber anisotropy, initial imperfections, voids and partial or complete slip at the fiber - matrix interface. For PRD-49-III unidirectional laminate, the compressive strength is of the order of 40 ksi (.275 GN/m^2) or only 20% of its tensile strength. Similarly, for composites made of Thornel 75S graphite fibers, the composite tensile strength in the fiber direction is of the order of 200 ksi (1.38 GN/m^2) while the compressive strength is only 80 ksi (.5515 GN/m^2). On the contrary, Boron-Epoxy composites have compressive strength of about 400 ksi (2.76 GN/m^2) and a tensile strength of about 180 ksi (1.24 GN/m^2). A commonly accepted failure mechanism of fiber reinforced materials subjected to compressive loads in the microbuckling of fibers. Analytical predictions of the compressive strength by such a mechanism were made by Rosen [4] and Schuerch [5]. Based on the results in References [4, 5], it is observed that the experimental correlation for Boron-Epoxy laminates is very good while there appears to be no correlation whatsoever for PRD-49-III laminates. Even for Thornel 50S graphite fibers, Greszczuk [6] noted that the discrepancy between theory and experiment is very wide. In essence, there remains some uncertainty associated with the lack of complete understanding of the mechanisms causing the relatively low compressive strengths of high modulus graphite, E-Glass and PRD-49-III composites.

A unique feature that distinguishes PRD-49-III fiber from Boron or E-Glass is its anisotropy. The axial shear modulus is less than 2% of the axial tensile modulus of the fiber. This is important not only because anisotropic fibers have not been considered in compressive strength analyses, but also because this means that the fiber axial shear modulus is of the same order of magnitude as the matrix shear modulus. A microbuckling analysis which takes into account the fiber anisotropy and slip at the fiber - matrix interface is presented in Chapter III.

An important aspect of this study is the experimental investigation of the compressive strength of PRD-49-III composites. Considerable experimental work related to the compressive strength of fiber reinforced composites appears to have been done. Schuerch [5] performed compression tests on Boron - Magnesium composites and showed that there is a good correlation with the microbuckling theory predicted by him particularly when inelastic behavior was assumed in the matrix. Lager and June [7] investigated the compressive strength of Boron - Epoxy composites. They suggested that an arbitrarily chosen influence coefficient of .63 can scale down the theoretical microbuckling analysis results so that they are in close agreement with the experimental results. Chung and Testa [8] also conducted tests on glass sheets reinforced

with resin and showed a fair agreement with their theoretical results. DeFerran and Harris [9] studied the behavior of polyester resin reinforced with steel wire. Their experiments yielded strengths well below the values predicted by microbuckling theory. They suggested that the fibers appear to buckle in a helical shape rather than into planar forms and it is likely that the lower elastic energy required for this deformation could be the reason for a poor correlation with the theoretical results. It was also observed in Reference [9] that fiber buckling was limited to a single shear zone. This type of failure is analogous to the dislocation controlled yielding spreading through a crystalline solid. Recently Greszczuk [6, 10] has conducted a study of the compressive strength of composites. The objective of the study in References [6, 10] was to establish the validity of the two dimensional microbuckling theory for high modulus graphite such as Thornel 50S composites and for two dimensional laminae. The conclusions of this study were: 1) actual composites made with Thornel 50S graphite fibers showed no evidence of microbuckling and macro- and microscopic observations confirmed this conclusion; the theoretical predictions were considerably higher than the experimentally obtained values, and (2) the transverse tensile strength of the composite affects the compressive strength significantly. Berg and Salama [11] have shown that fracture surfaces produced by compressive fatigue of Celanese GY70 fiber reinforced composites indicate that microbuckling, in the form of kink band formation is the principal mechanism of notch extension. Argon [12] has cited a kinking collapse mode of compressive failure in Boron-polyimide-epoxy fiber laminate. Initial misalignment of the fiber was attributed to this form of failure.

Experimental studies not necessarily in the context of microbuckling theory have also been performed. Davis and Zender [13] performed compressive tests on E-Glass epoxy plates and Davis [14] studied the compressive instability of S-Glass and Boron-epoxy tubes. It is seen from the results of Reference [14] that with carefully made test specimens of Boron-epoxy, it is possible to achieve the strength values predicted by the microbuckling theory. Thus, a wide range of tests have been performed and it is evident that the conclusions arrived at are at times confusing, and conflicting. Also, none of these are for PRD-49-III fibers. It is believed that the present experimental program confirms some of the observations of the previous studies and provides additional information concerning the mechanism of compressive failure.

There are a number of compression test methods available, viz., ASTM, Celanese, tube and honeycomb sandwich. Compression tests performed on any given composite using two different test methods show substantial differences in result. Hence, the first phase of the experimental program consists of a comparative evaluation of various compression test methods. Unidirectional E-Glass and PRD-49-III composite test specimens

were prepared for four different test methods, viz., ASTM stabilized flat plate, Celanese flat plate, honeycomb sandwich and short circular tube. The results were compared with available results in the literature. On the basis of these results, a basic specimen which indicated the lowest standard deviation was defined for use in the following phases of the program. Results of the first phase appear in Chapter IV.

The second phase of the experimental program consisted of the following variations of various factors that might affect the compressive strength:

1) Alteration in fiber physical and surface characteristics before resin impregnation:
   a) Pretension;
   b) Pretwist;
   c) 'Teflon' coating;
   d) 'Moisture' coating;
   e) Increased yarn diameter;

2) Introduction of lateral reinforcement:
   a) 0° - 90° Glass cloth;
   b) $\pm$45° Glass cloth;

3) Alteration of the physical and mechanical properties of the matrix;
   a) Low viscosity dilute resin;
   b) Flexibilized resin with a high strain to failure;
   c) Low temperature cured resin;
   d) High temperature post cured resin;
   e) Resin filled with Aluminum metal dust;
   f) Resin filled with Alumina particles;
   g) Resin filled with Iron Oxide particles;

4) Off-axis laminae at small $\pm\theta$° orientation.

Salient features of this phase of the study are discussed in Chapter V.

It was subsequently observed that the alteration of the abovementioned variables did not result in an appreciable increase in the compressive strength. However, a noticeable increase in the compressive strength and a change in the mode of failure was observed for the 0° - 90° glass cloth reinforced specimens. This gave credence to the belief that transverse strength of the composite may have an important effect on the longitudinal compressive strength. Hence, it was decided to

explore the compressive strength of a PRD-49-III composite reinforced by PRD-49-III fibers in the transverse direction. Also, consideration of the fact that 'Teflon' and moisture coating did not decrease the compressive strength appreciably as compared to the control specimen and that the failure always resulted from the formation of shear bands either in the plane of loading or the transverse plane prompted Scanning Electron Microscope studies of the shear band failures of the specimens. Such an investigation would confirm the existence of slip planes within the fiber, nature of the post failure mechanism in the fiber and the existence of (or the absence of) fiber-matrix bond. Confirmation of slip bands in the individual fibers and the poor bond between fiber and matrix suggested that the highly oriented polymer fibers are inherently weak in compression and in order to overcome the disadvantage, hybrids, or multiple fiber reinforcements should be actively considered. The various aspects discussed above are presented in detail in Chapter VI.

Finally, conclusions are drawn and recommendations made for future investigations in the field of compressive strength of anisotropic fibers in Chapter VII.

III. MICROBUCKLING OF ANISOTROPIC FIBERS IN FIBER-REINFORCED COMPOSITES

Microbuckling as a failure mechanism in fiber-reinforced composites was suggested first by Dow and Gruntfest [15] and observed by Rosen [4] for single E-Glass filaments embedded in blocks of epoxy which were cooled to produce a compressive strain in the filaments. Subsequently, analyses of this form of instability were performed, independently, by Rosen [4] and Schuerch [5]. The fiber-reinforced composite was modelled as a layered two-dimensional medium wherein the fiber and the matrix represented a repeating pair of layers. The fibers were assumed to buckle sinusoidally. When adjacent fibers buckled 180° out of phase with each other as in Figure (1a), the matrix behaved as a tension-compression foundation and this mode of buckling was termed as extensional; when they buckled in phase as in Figure (1b), the major strains in the matrix are shear strains and as a result, this mode was denoted as a shear mode. The critical composite stress obtained by Rosen [4] for the extensional mode was

$$\sigma_{c(E)} = 2v_f\left(\frac{v_f E_m E_f}{3(1-v_f)}\right)^{1/2} \qquad (1)$$

while that obtained by Schuerch [5] was

$$\sigma_{c(E)} = 2v_f \left[\frac{v_f E_m E_f}{3(1-v_f)}\right]^{1/2} \left[1 + \frac{(1-v_f)E_m}{v_f E_m}\right] \tag{2}$$

where v_f = fiber volume fraction,

E_m = modulus of elasticity of matrix,

and E_f = modulus of elasticity of fiber.

For most composites, $E_m/E_f << 1$. Hence, Equation (2) reduces to Equation (1). For the shear mode, the results in References [4, 5] were identical and the critical compressive stress is

$$\sigma_{c(s)} = \frac{G_m}{(1-v_f)} + \frac{\pi^2 v_f E_f}{12} \left(\frac{nh}{\ell}\right)^2 \tag{3}$$

where G_m = matrix shear modulus,

n = wave number,

h = fiber diameter or reinforcement thickness,

and ℓ = length of composite specimen.

If the buckle wave length ℓ/n is large compared with the fiber diameter, the second term in Equation (3) can be neglected and the composite buckling stress is given approximately by

$$\sigma_{c(s)} = \frac{G_m}{(1-v_f)} \tag{4}$$

It was pointed out in References [4, 5] that for $v_f < .2$, the extensional mode would predominate while the shear mode will prevail for $v_f \geq .2$. This form of shear instability caused by compressive loads has also been observed for wood and polyurethane foam by Hayashi [16].

Chung and Testa [8] also investigated the microbuckling of fibers by the theory of generalized plane stress. The governing equation of equilibrium were those for a medium under initial stress as formulated by Biot [17]. The critical buckling stresses as obtained in [8] reduced to Equation (1) and (8) for buckle wave length large as compared to fiber spacing and $\nu_m = 0$. Various other analytical solutions have been

presented by Sadowsky et al [18], Hermann et al [19] and more recently by Lanir and Fung [20]. Unfortunately, these solutions are for single fibers embedded in a matrix and hence, do not represent appropriately the true behavior of fiber-reinforced composites. A review of the theories of microbuckling appearsin Reference [10].

The critical buckling stresses obtained in all the above-mentioned studies assume that the fiber is isotropic and that $G_f >> G_m$. Hence, the critical buckling stress in Equation (4) for the dominant shear mode is not a function of the fiber constituent properties. For anisotropic fibers like PRD-49-III or Graphite, G_f and G_m are of the same order. So the shear deformation in the fiber should be considered. The effect of fiber anisotropy which is reflected in the E_f/G_f ratio was considered in a rather approximate fashion by Greszczuk [6]. Greszczuk [6] incorporated the shear deformation effects in the fiber by modifying the column buckling term in Equation (3) which was rewritten as

$$\sigma_{c(s)} = G_{LT} + \frac{\pi^2 v_f E_f}{12}\left(\frac{nh}{\ell}\right)^2 \left[\frac{1}{1+\frac{\kappa\pi^2 E_f}{G_f}\left(\frac{h}{\ell}\right)^2}\right] \qquad (5)$$

where κ = value of the shear coefficient which depends upon the cross-sectional shape, and it was assumed that $G_m/(1-v_f)$ represents the shear modulus G_{LT} of a two dimensional model composite. The actual value of G_{LT} as obtained from a three-dimensional micromechanics analysis is greater than $G_m(1-v_f)$. However, it should be expressly mentioned here that the substitution in Equation (4) for $G_m/(1-v_f)$ by G_{LT} as obtained from the three dimensional michromechanics analysis for a two dimensional composite is questionable. It is proposed here to extend the existing two dimensional model to include the effects of shear deformation and fiber anisotropy. This would appropriately alter the value of G_{LT}.

Referring to Figure (1b) and invoking the shear stress continuity and strain compatibility at the fiber-matrix interface, it can be shown that the shear deformation in the fiber due to τ_{xy} is

$$\alpha_f = u_{y,x} \frac{g_1}{1+g_2} + \gamma_f \frac{g_2}{1+g_2} \tag{6}$$

where $g_1 = \frac{G_m}{G_f}(1+\frac{h}{2c})$, $g_2 = \frac{G_m}{G_f}\frac{h}{2c}$ and γ_f is the bending shear strain defined by:

$$\gamma_f = \kappa \frac{h^2}{12} \frac{E_f}{G_f} u_{y,xxx} \tag{7}$$

The shear strains are assumed to be a function of the longitudinal coordinate only. The transverse displacement u_y is independent of the transverse coordinate and each fiber is assumed to buckle in a sinusoidal pattern expressed by the following series:

$$u_y = \sum_n A_n \sin \frac{n\pi x}{\ell} \tag{8}$$

The total change in the strain energy of the fiber ΔV_f comprises of the changes in the bending strain energy and the shear strain energy due to the rotations α_f and γ_f. Hence, following the procedure in Reference [4],

$$\Delta V_f = \frac{\pi^4 E_f h^3}{48\ell^3} \sum_n n^4 A_n^2 (1+f_n) + \frac{G_f h}{2(1+g_2)^2} \sum_n (g_1 - g_2 f_n)^2 \frac{n^2\pi^2}{2\ell} A_n^2 \tag{9}$$

where $f_n = \frac{\kappa n^2 \pi^2 h E_f}{12 \ell^2 G_f}$.

The total change in the shear strain energy of the matrix is:

$$\Delta V_m = \frac{c G_f^2}{G_m (1+g_2)^2} \sum_n (g_1 - g_2 f_n)^2 \frac{n^2 \pi^2}{2\ell^2} A_n^2 \qquad (10)$$

The work done by the externally applied load as the composite changes from a compressed but unbuckled configuration to the buckled state is:

$$\Delta T = \Delta V_m + \Delta V_f = \frac{\sigma_f h \pi^2}{4\ell} \sum_n n^2 A_n^2 \qquad (11)$$

Substituting the values for ΔV_f and ΔV_m from Equations (9) and (10) respectively, the fiber stress is:

$$\sigma_f = \frac{\left[\frac{\pi^2 E_f h^2}{12\ell^2} \sum_n (1+f_n) n^4 A_n^2 + \frac{G_f}{(1+g_2)g_2} \sum_n n^2 A_n^2 (g_1 - g_2 f_n)^2\right]}{\Sigma n^2 A_n^2} \qquad (12)$$

If σ_f is a minimum for a given value of n, then

$$\sigma_{f(s)} = \frac{G_f}{(1+g_2)g_2} (g_1 - g_2 f_n)^2 + \frac{n^2 \pi^2 E_f h^2}{12\ell^2} (1+f_n) \qquad (13)$$

Assuming once again that $\ell/n >> h$, the critical composite buckling stress for the shear mode is

$$\sigma_{c(s)} = \frac{G_m}{(1 - v_f + G_m v_f / G_f)} \qquad (14)$$

where $v_f = \frac{h}{h+2c}$. It is evident that for $G_m/G_f << 1$, Equation (14) reduces to Equation (4). Also, the expression for $\sigma_{c(s)}$ in Equation (14) is bounded for values of v_f near unity unlike that in Equation (4).

Figure (2) shows the variation of the critical fiber buckling stress with matrix shear modulus for different volume fractions of PRD-49-III fiber. For a matrix shear modulus of 200 ksi (1.38 GN/m^2), the value predicted by Equation (14) is 390 ksi (2.68 GN/m^2) while that obtained from Equation (4)

is 830 ksi (5.72 GN/m^2). Thus, there is a decrease in the value of the critical fiber stress when the shear deformation in the fiber is considered. Unfortunately, the result is higher than the experimental figure of 40 ksi (.275 GN/m^2) by an order. Hence, it is necessary to consider additional effects that lead to a deterioration of the compressive strength such as initial misalignment of the fiber, presence of voids and slip at the fiber matrix interface. Though the effect of the initial misalignment of the fiber can be incorporated in a straight forward manner, there remains the question of the variation of misalignment of fiber in each specimen. Based on the analogy of kink bands in metal crystals, the compressive strength of the composite was obtained by Argon [12] to be

$$\sigma_c = \frac{\tau}{\phi_o} \tag{15}$$

where τ is the interlaminar shear strength and ϕ_o is the initial misalignment. However, the value of ϕ_o may be quite arbitrary and as such, the results of Equation (15) may be unreliable. Foye [21] performed a macroscopic analysis to permit a rough estimation of the influence of fillers and voids on the compressive strength. It was concluded in Reference [21] that void content can reduce the compression resistance particularly at high reinforcement contents. Also, only marginal gains in the compression strength are derivable from small amounts of powdered matrix additives.

The degrading effect of an imperfect bond between fiber and matrix can be estimated by considering the case of the shear mode microbuckling for the two dimensional model. By assuming that the buckling mode displacements in the matrix are

$$U_x = k\frac{h}{2c}\frac{du_y}{dx}\left[y-\left(\frac{h}{2}+c\right)\right] \tag{16}$$

as in Figure (1c), the amount of slippage between fiber and matrix is included through the parameter k. For a perfect bond, k = 1; for no bond, $k = -\left(\frac{1-v_f}{v_f}\right)$.

Equating the change in the stored energy in the matrix to the change in the potential energy of the applied load and following Rosen [4], the compressive strength for the fibrous composite is given as

$$\sigma_{c(s)} = \frac{G_m[1-(1-k)v_f]^2}{(1-v_f)} \tag{17}$$

where $-\left(\frac{1-v_f}{v_f}\right) \leq k \leq 1.$

Figure (3) shows a graph of this compressive strength for a matrix shear modulus of 200 ksi (1.38 GN/m^2). Although no quantitative conclusions should be drawn from Figure (3), the possible degrading influence of the interface condition upon the compressive strength is evident. For example, for $v_f = .6$, the partial slip case of $k = 0$ is 16% of the no slip value, that is, 80 ksi (.55 GN/m^2) versus 500 ksi (3.44 GN/m^2).

Considering the previous analysis concerning anisotropic fibers and introducing the possibility of slip as above, Equation (14) is modified to:

$$\sigma_{c(s)} = \frac{G_m[1-(1-k)v_f]^2}{(1-v_f+G_m v_f/G_f)} \tag{18}$$

where k is restricted such that $-\left(\frac{1-v_f}{v_f}\right) \leq k \leq 1.$

Considering the case where $G_m = G_f = 200$ ksi (1.38 GN/m^2), $v_f = .6$ and partial slip ($k=0$), the compressive strength becomes 6.4% of the isotropic fiber no-slip condition, that is, 32 ksi (.22 GN/m^2) versus 500 ksi (3.44 GN/m^2).

The expression for $\sigma_{c(s)}$ in Equation (14) is identical to the Reuss estimate of the longitudinal-transverse shear modulus G_{LT} of a unidirectional composite. The Reuss estimate is a 'stiffness in series' model. Thus, it seems that the shear modulus of a composite is the critical composite buckling stress. This has been proposed by Leonard [22] for woven fabrics and by Foye [21] for composites. In fact, if one were to consider a unit element of a two dimensional sheet subjected to a compressive stress σ_c and subsequently subject it to a planar shearing stress τ, the following modified stress strain law will be obtained (for small shear angle γ)

$$\tau = (G_{LT}-\sigma_c)\gamma \tag{19}$$

The term $G_{LT} - \sigma_c$ may be termed as the effective shear modulus and for $G_{LT} = \sigma_c$, there is a complete loss of shear stiffness. As is evident, the effective shear modulus is not a basic material property but merely a function of the state of stress. It is interesting to observe that Biot [17] has shown that for an elastic body under prestress, the elastic constants are not the same as in the unstressed condition unless the prestress system is hydrostatic. For the abovementioned two dimensional model, σ_c is the prestress which effectively changes the shear modulus.

It can thus be summarized that the theoretically calculated composite buckling stress is indeed an estimate of the shear modulus. However, this value of the buckling stress (even with the inclusion of fiber anisotropy) is almost an order higher than the experimentally obtained value for PRD-49-III composites. Partial interfacial slip reduces the buckling stress considerably. Consideration of additional effects of fiber misalignment and voids will further reduce its value. However, in order to justify theoretically a value of about 40 ksi (.275 GN/m^2), the fiber must have a predetermined misalignment and interfacial slip. Findings from the experimental investigation carried out here fail to reinforce the concept of a predetermined slip or misalignment.

IV. SELECTION OF TEST SPECIMEN CONFIGURATION

The problems associated with the compression test methods are well known. Two major obstacles that must be overcome are: 1) end effects such as end brooming giving rise to a shaving brush like appearance, uneven bearing or contact surface, introduction of lateral shearing stresses leading to premature failure because of low axial shear stiffness of composites, end buckling of fibers and splitting and high shear and moment gradients such as in tubes; 2) specimen instability. The following test methods are generally used:

1) ASTM 'dog bone' Stabilized Specimen: This method is described in Reference [23]; this test might yield high strengths by providing a higher restraint within the stabilizing fixture; alternatively, failures between the fixture and the loading head produce lower results because of splitting, end brooming and delamination. However, this is a relatively simple test and inexpensive to perform.

2) Honeycomb Sandwich: Features of this method are discussed in Reference [24]. The modes of failure associated with this specimen are column buckling, shear crimping, filament fracture, layer instability, face wrinkling and dimpling and end crushing. The problem of end failure can be avoided by end potting and/or loading caps.

3) Short Circular Tube: The short circular tube has been used for determining the compressive strength of unidirectional composites by Davis [14] and its application to biaxial loading has been investigated in Reference[24]. The major problem with this test method is edge effects. This problem has been addressed to Pagano and Whitney [25] and Miller [26] Also, the fabrication involves a complex procedure and is costly.

4) Celanese Specimen: This is a short column test restrained against instability by grips. A description of test procedure and fixture is given in Reference [27]. Disadvantages of this test are the non-uniform transfer of shear stress from the grips to the specimen, possibility of column type buckling when tabs are used and debonding of tabs from the specimen.

5) TEI Short Column Specimen: This test method developed by Texaco Experimental Inc. [24] requires no supporting device. However, the penalty of using short specimens is twofold: a) end effects may occupy a significant portion of the test length, and b) the detrimental effect of incomplete contact at the ends. Daniels [28] has suggested a modification of the TEI set up.

Considering the advantages and disadvantages of each method, it was decided to fabricate samples for the ASTM, Celanese, Circular Tube and Honeycomb Sandwich test methods from commercially available E-Glass and PRD-49-III prepregs. The dual purpose of this initial phase of the study was:

1) evaluate the correlation of available test data and the present experimental data, and

2) determine which test method gives the least scatter.

On the basis of these results, one or two basic test specimen configurations will be utilized for the study of the compressive strength of PRD-49-III laminates in the subsequent phases. Tables III and IV give the description of the first phase specimens and Tables V through XIV the results obtained for these tests.

Anticipating for PRD-49-III test coupons a strength of 40 ksi (.275 GN/m^2) and a standard deviation of 1 ksi (.0069 GN/m^2), it was determined that 5 tests for each variation will give a 95% confidence level. Hence, 5 test specimens were fabricated for each material system.

In Figure (4) are shown the modes of failure for the E-Glass specimens. For the ASTM specimen no. 4, the failure is due to end delamination and longitudinal splitting. The end delamination results from improper contact with the machine head as discussed earlier. Two thicknesses for the ASTM specimens were tested and it is seen from Tables V and VI that the smaller thickness yielded a lower average value. In fact, the .11 in. (2.79 cm.)

nominal thickness samples gave an excellent correlation with the 3M value of 90 ksi. (.62 GN/m^2).

Both tabbed and untabbed specimens were tested in the Celanese test fixture. However, only the tabbed specimen values are shown in Table VII because the untabbed samples exhibited a wide scatter of compression strengths. This was mainly because of uneven gripping which could be easily seen from the teeth marks on the specimen faces. The tabbed specimen gave more uniform results though in one case, the tabs were separated from the specimen. The higher results for some samples could be attributed to improper collimation between the tapered sleeve and the outer cylindrical shell portion of the Celanese test fixture. Crumpling and splitting of fibers was the predominant failure mode.

The short circular tubes were fabricated in a manner similar to one outlined by Davis [14]. The results for the short circular tube with end loading caps are tabulated in Table VIII. The average compressive stress is in good agreement with the documented value. The mechanism of failure was end brooming and longitudinal splitting. Specimen No. 24 in Figure (4) apparently indicates a column type buckling but it could as well be a post failure mechanism.

For the sandwich facings, Scotchply 1002 prepreg was used. The face sheets were cured at 330° F for 1/2 hr. and subsequently post cured at 280°F for 16 hrs. The honeycomb cores were made from 5056 Aluminum, .125 in. (3.175 cm.) cell, .002 in. (.05 cm.) gage, .5 in. (12.7 cm.), 8.1 pcf (.136 gm/cc) Aluminum honeycomb. Pieces of honeycomb were cut 4.5 in. (.11 m) x 13 in. (.33 m) with the honeycomb ribbon running in the 4.5 in. (.11 m) direction. Cells of these pieces were filled with liquid Epon 815 epoxy resin across the 4.5 in. (.11 m) direction. Starting at one end, 1 in. (25.4cm) was filled, 2 in. (50.8 cm) left empty, etc. The 1 in. (25.4cm) filling corresponded to the end potting. The resin filled honeycomb was cured at room temperature and post cured at 250°F for 1 hr. The laminate faces were then bonded to the honeycomb core using Hysol epoxy film. The sandwich was cured in vacuum bag at 250°F for 1 hr. 1 in. (25.4cm) x 3 in. (76.2cm) test samples were then cut so that there were .5 in. (12.7 cm) of epoxy filled honeycomb cells at each end of the test coupon underneath the faces.

The sandwich specimens generally indicated rather complex modes of fracture simultaneously such as separation from the core, core failure and filament or matrix fracture. It must be recalled the samples are end potted and the load is transmitted through end blocks. Hence, the presence of slight bending in the sample will result in stress concentration at one of the free edges of the end block and the face sheet and subsequent fiber or matrix failure. This is confirmed in Figure (4) for sample no. 32. Probably because of this, the average compressive

stress is about 10% lower than 90 ksi (.62 GN/m^2).

The summary of the abovementioned compressive test appears in Table XV. It is immediately obvious that the sandwich test has the lowest standard deviation followed by the ASTM sample. The sandwich average compressive strength is however lower than the ASTM flat plate. The Celanese and the tube show a very high scatter.

The PRD-49-III first phase samples were fabricated from Scotchply SP-306 prepreg. The SP-306 face sheets were cured at 350°F for 2 hrs. and post cured at 400°F for 16 hrs.

The failure modes for these specimens are illustrated in Figure (5). The ASTM samples, .104 in. (2.64 cm) and .055 in. (1.39 cm) thick, invariably showed the formation of shear bands emanating from the edges. For the .104 in. (2.64 cm) thickness flat plate, no longitudinal splitting or end brooming was observed. This was definitely a unique feature. For the .055 in. (1.39cm) specimen, however, some end delamination and longitudinal splitting was evident mainly because of the difficulty associated with a smaller loading area. The results for the two tests are shown in Tables X and XI. As for E-Glass, the larger thickness specimens yielded higher compressive strengths. The average compressive strength from Table X is 35.61 ksi (.245 GN/m^2) while the generally accepted value is about 40 ksi (.275 GN/m^2) for a fiber volume fraction of .6. However, the fiber volume fraction for SP-306 varies from .55 to .6 and hence the lower compression strength may not have any special significance.

The Celanese tests presented the same problems as before. The application of shear loading by means of grips was non-uniform. Also, for some samples, the compression strengths were in excess of 45 ksi (.31 GN/m^2) alluding to the fact that part of the applied load is transferred from the tapered sleeve to the outer cylindrical shell. The failure was mainly due to a combination of shear band and inter - layer delamination. The shear bands were not as obvious as in the ASTM tests and the layer separation could be attributed to thickness effects. The post failure mechanism was a bulging out of the test section and no fiber break was visible - unlike E-Glass, Graphite or Boron. This bulge is seen for specimen no. 54 in Figure (5). For a PRD-49-III woven cloth laminate, shearing in the form of kinking is very obvious. This is also shown in Figure (5). A similar form of failure has been mentioned by Argon [12]. The average ultimate compressive stress obtained was higher than the ASTM case.

The circular tube tests were very poor as can be seen from Table XIII. The reason for the poor results is the inherent weakness of the tube as a compression test specimen because of the existence of edge effects leading to high circumferential strains and possible inter - layer delamination.

Finally, the sandwich specimen again confirms the shear band type failure with bands originating at the edges. The failure in the core was conspicuously absent and there was no evidence of fiber fracture as in E-Glass. The average compressive strength in Table XIV is 36.13 ksi (.249 GN/m^2) and at this stage the sandwich appears to be the best test specimen - not considering the cost and difficulties involved in fabrication.

A summary of the first phase test results for PRD-49-III is given in Table XVI. The ASTM and Sandwich are the most attractive candidates considering not only the strengths but also the low scatter. Consideration of the fact that sandwich construction is frequently used in aerospace application influenced the decision to fabricate sandwich samples for the subsequent experimental program. However, the ASTM specimen was not entirely ruled out and as can be seen in the later part of this report, was frequently employed to confirm results obtained from the sandwich.

V. MECHANICAL SCREENING TESTS TO STUDY PROCESS PARAMETERS

With the basic specimen configuration defined, the second phase of this study consists of various alterations of the physical and mechanical properties of the constituents (matrix and PRD-49-III fiber) and the addition of lateral reinforcements and to observe their effect on the ultimate compressive strength of unidirectional PRD-49-III laminates. To this effect, the task was divided into the following categories:

1) Addition of lateral reinforcement:
   a) 0° - 90° Glass cloth between PRD-49-III laminae;
   b) ±45° Glass cloth between PRD-49-III laminae;
   c) PRD-49-III fibers in transverse directions;
2) Change in the physical properties of fiber:
   a) Pretensioning of fiber;
   b) Pretwisting of fiber;
   c) Increasing fiber tow diameter;
   d) Coating fiber with 'Teflon';
   e) Coating fiber with moisture.

3) Alteration of mechanical and physical properties of the matrix:

   a) Reinforcement of matrix by Alumina Powder;

   b) Reinforcement of matrix by Iron Oxide Powder;

   c) Reinforcement of matrix by Aluminum metal dust;

   d) Low Temperature Cured Resin;

   e) High Temperature Cured Resin;

   f) Low Viscosity Dilute Resin;

   g) Flexibilized Resin.

4) Off-axis laminae at small $\pm\theta°$ orientation.

5) Blend of PRD-49-III/HTS laminates.

Since a variation of the fiber and matrix properties was involved, the fabrication of the honeycomb sandwich specimen was done at the DuPont Experimental Station. A commercially available resin such as American Cynamid BP-907 resin was used instead of PR-286 which is used in Scotchply SP-306. Hence, it was necessary to define a control sample with BP-907 resin. Physical and mechanical properties of BP-907 resin are tabulated in Table XVII. The fabrication procedure is briefly described here. The preparation procedure consisted of filament winding of PRD-49-III yarn around a thin rectangular plate covered with 'Teflon' release film. Epoxy resin was applied either by passing the yarn through a 15% BP-907/ethylene dichloride liquid dip or by applying BP-907 film to layers of fiber after they were wound onto the 'Teflon' coated plate. The laminate was then cured at 350°F in vacuum bags in autoclave at 100 psi (.00069 GN/m^2) for 2 hrs. The filament winding apparatus consisted of:

1) Bobbin of yarn placed on triple beam balance for determination of amount of yarn used in laminate;

2) A tension gate for applying uniform tension during fabrication;

3) A dip tank if liquid resin was used;

4) A card winder for filament winding of the yarn on a 'Teflon' film covered 13 in. (.33 m) x 5 in. (.127 m) x .125 in. (3.175 cm) plate;

5) Appropriate yarn guides and rollers.

After curing, both ends of the laminate were ground away and subsequently, the laminate was removed. The cured sheets (one on each side) was 4.5 in. (.114 m) wide and 13 in. (.33 m) long.

The preparation of the honeycomb core and the bonding of face sheets to core was performed in a manner already outlined in the earlier chapter. Description of the various specimens is given in Tables XVIII through XXII.

The control specimen failure is shown in Figure (5) and the test results are tabulated in Table XXIII. Because of improper machining of the samples at the potted end, the potting was removed for some specimen and hence only four undamaged specimens were tested. Since the least number of specimens to be tested was five for a certain confidence level, another series of ASTM control specimens was fabricated. The purpose for the fabrication of the ASTM specimens was to study the following aspects:

1) How much of an alteration would occur in the ultimate compressive stress with a change in specimen geometry?

2) In Figure (5), the shear bands for sample Nos. 73 and 102 tend to follow the honeycomb cell boundaries; hence it is essential to know whether the inclination of the slip plane is adversely affected by the lateral constraint provided by the honeycomb.

Referring to Tables XXXIX which gives the fiber failure stress based on the rule of mixtures (not necessarily an accurate method to determine fiber stress), it is seen that the ASTM specimen yields a slightly lower value. However, the failure mechanism is similar, i.e., a shear band at the same inclination. The load displacement curve for the control sandwich specimen No. 107 is shown in Figure (6).

The effect of the addition of lateral reinforcements is studied next. The lateral restraint was provided by 0° - 90° and ±45°, Style 106 Glass fabric. These specimens were prepared by altering plies of Scotchply SP-306 prepreg and Glass fabric to obtain the desired thickness. The results are given in Tables XXV and XXVI. At the outset, it is obvious from Table XXXIX that the compression strength has increased for the 0° - 90° Glass fabric reinforcement while that for the ±45° reinforcement has not altered. Three important observations must not go unnoticed. They are:

1) The increase in strength could be possibly attributed to the additional glass reinforcement in the 0° direction.

2) The lateral restraint provided by Glass in the 90° direction results in a change in the failure mode. Instead of having the slip plane in the plane of the loading which involves a lateral slip, the slip is in a transverse plane. This is illustrated in Figure (7) for specimen No. 115. Also, longitudinal splitting is inhibited. The slip in the transverse plane occurs because there is no reinforcement in the thickness direction. So if a transverse reinforcement is provided in the thickness direction, the shear band type failure can possibly be eliminated and a much higher strength will result. In fact, Table XXV indicates that

two specimens show no evidence of shear failure and the ultimate load corresponded to shear crimping and separation of face sheets from core.

3) It seems at this stage that the transverse tensile strength plays an important role in the longitudinal compressive strength. This has been pointed out by Greszczuk [6] and Chamis [29]. Whether this is indeed true or not will be confirmed by providing additional transverse reinforcements in the form of smaller diameter PRD-49-III yarn in lieu of 0° - 90° Glass fabric.

For the ±45° Glass fabric reinforcement, on the contrary, the results are not encouraging. The failure mode is not altered and the shear bands tend to follow the weakest plane, i.e., at ±45°. The presence of vertical cracks in sample No. 121 is not surprising because the transverse tensile strength contribution of ±45° Glass fabric is minimal as compared to the 0° - 90° Glass fabric. In fact, the only advantage provided by ±45° Glass fabric is a possible increase in the shear modulus. But this increase is in no way reflected in the compressive strength. This suggests no relationship of shear modulus with ultimate compressive stress as far as PRD-49-III composites are concerned.

Figure (8) shows a plot of the load displacement curve for the 0° - 90° and ±45° Glass fabric reinforced specimens. The proportional limit is the same for both types of the reinforcements and the nature of the curves is bilinear. The additional strength is derived from the portion of the curve beyond the proportional limit.

The next part of this phase involved the variation of the PRD-49-III fiber physical properties. The effect of initial pretension was investigated first. A 125g tension was applied during winding. After curing on the card winder, both ends of the cured laminate are ground away. This will induce a residual compressive stress in the resin. Referring to Table I, the axial thermal coefficient the expansion of PRD-49-III fiber has a small negative value while the average value in the radial direction is 205×10^{-6} in./in., °C. The corresponding value for BP-907 resin is only $25\text{-}40 \times 10^{-6}$ in./in., °C. These figures indicate that during curing, the shrinkage will be greater for the PRD-49-III fiber and unless the surface tension between the resin and fiber is high enough, the fiber may not have a good bond at all. In this context, a pretensioning of the fiber will be of no avail. Results in Table XXXIX actually indicate a drop in the compression strength. The failure mode is illustrated in Figure (9) for specimen No. 135 and the results of the test are tabulated in Table XXVII. The nature of the load displacement diagram for specimen no. 131 in Figure (10) is similar to the control specimen.

The effect of pretwist was investigated subsequently. A twist of 2 TPI (Turns per Inch) was applied during winding. Generally, the effects of pretwist are detrimental as far as the compressive strength is concerned because the effect of pretwisting is equivalent to a misalignment of the fiber. As can be seen from Table XX, two specimen types were fabricated. This was because of the fact that an erroneous calibration of the load cell gave unreliable results for the sandwich series 141-150. Subsequently, the ASTM series 141C-150C was fabricated. Noting that the fiber volume fraction for the ASTM specimens was .635, it is obvious that the average compression strength of 35.59 ksi (.2454 GN/m^2) in Table XXVIII indicates a decrease. Because of the changing orientation of the fiber axis with respect to the direction of loading, the slip plane is not continuous. This can be seen from Figure (9). Also, as a result, the angle of the slip plane is different from the normal value of 55°-60°. Longitudinal splitting is also observed. For specimen No. 144 in Figure (9) a split served to connect two shear bands at different location with each band covering the width of the specimen not covered by the other. Surprisingly, the load deformation curve in Figure (10) indicates considerable activity in the inelastic region.

The effect of increasing the yarn diameter to 1140 Deniers from 380 Deniers was considered next. No appreciable change in the strength is observed in Table XXXIX. However, the region of shear damage seems to diffuse and spread over a wide region. This is evident for specimen No. 224 in Figure (9). Note also the departure in the load displacement curve for the same specimen from the control in Figure (6).

The possibility of a poor bond between fiber and matrix has already been discussed. However, it was decided to purposely attempt to destroy the interface bond by coating the fiber with 'Teflon' and moisture. 'Teflon' was applied to the PRD-49-III yarn by passing yarn through a bath containing 'Teflon' release agent. Fiber was then dried to determine 'Teflon' pick up prior to wet winding with 15% BP-907/ethylene dichloride solution. 'Teflon' was applied at room temperature. It must be remembered that 'Teflon' is in a suspension form and passing yarn through the 'Teflon' release agent will not guarantee a smooth coating of 'Teflon' on the fiber surface. In fact, the SEM photo-micrographs in Chapter VI show no evidence of a 'Teflon' coating. So the 'Teflon' particles are probably dispersed on the fiber surface unevenly and hence, the interfacial bond is not completely destroyed. In order to obtain a continuous film over the fiber surface, the temperature must be raised to a certain level. At that level, the fiber loses its integrity. The average compressive strength for the 'Teflon' suggests a decrease while for the moisture coating no change is noticeable in Table XXXIX. Longitudinal splitting and shear bands are visible for specimen nos. 237 and 244 in Figure (9). The nature of the load deformation curves as illustrated in Figure (11) is almost similar for both specimen types.

As is apparent in the microbuckling results obtained by Rosen [4] and is suggested by Foye [21], the shear buckling mode is a function of the matrix shear modulus. With the assumption that this is true, it is appropriate to consider the various alteration in the matrix properties which will increase its modulus of elasticity, compressive strength and strain to failure. To translate the changes in the matrix mechanical properties into the properties of the composite is not always possible and a priori assessment of the matrix contribution to the composite strength must be done with great care. In a recent study, Chamis [29] has observed from a phenomological point of view that 1) the area under the stress-strain curve bounded by 1% strain is a good indicator of the matrix contribution to the composite properties and strength; 2) matrix modulus is the governing parameter for the compressive strength and 3) the matrix ultimate strength and elongation are not suitable parameters to correlate composite strength with matrix properties.

The matrix modulus and comprssive strength were changed by the addition of fillers. The effect of fillers on the matrix properties has been assessed by Dow and Rosen [30], in Reference [31] and mentioned by Foye [21]. Three fillers were used, viz., Alumina, Iron Oxide and Aluminum metal dust. The effect of all these fillers is to increase the resin modulus. The increase is highest for Alumina followed by Iron Oxide and Aluminum metal dust. However, the compressive strength actually decreases for Aluminum metal dust and increases for Alumina and Iron Oxide. Hence, the percent weight of fillers in the matrix were chosen such that:

1) the compressive strengths of Iron Oxide and Alumina reinforced resins are identical; and

2) the modulus of Alumina and Aluminum metal dust filled matrix are the same; however, the modulus for the matrix with Iron Oxide filler is higher.

Thus, if the compressive strength of the matrix influences the compressive strength of the composite, Iron Oxide and Alumina fillers should yield a higher value. If the modulus, and hence the shear modulus, affects the compressive strength, then Alumina and Aluminum metal dust reinforced specimens should yield almost similar ultimate compressive stress and the Iron Oxide, a higher value. The solid particulate additives were dispersed in the liquid resin in the dip tank and the dispersion was kept agitated during winding. Referring to Table XXXIX, the Alumina and Iron Oxide specimens indicate an increase and the Aluminum metal dust suggests no change in the fiber compressive stress. However, based on practically attainable fiber volume fractions in filled matrices, the composite strength may not reflect an increase and an increase or decrease in the fiber compressive stress should be viewed in the proper perspective. These results also suggest that the increase in the matrix modulus by the addition of fillers have not increased the composite strength

as suggested by Equation (4) of Chapter III. The nature of the failure for these specimens is shown in Figure (12) and the load displacement plots in Figure (13). Note that for equal fiber volume fraction as in Alumina and Iron Oxide filled composite specimens, the load at proportional limit is not altered. This is analogous to the 0° - 90° and ±45° Glass cloth reinforced specimens.

The effect of the curing cycle should be felt on the ultimate strain to failure of the matrix and the residual interface stresses. Two curing temperatures and times were used. They are: 1) 250°F, 95 hrs., and 2) post cure at 400°F, 16 hrs. Both samples registered a decrease in the compressive stress. However, the high temperature cured resin indicated a substantial drop in the strength and the reason for this deterioration is the brittle nature of the cured resin. Though shear bands did appear, considerable longitudinal splitting also occurred. This can be seen in Figure (12) for sample No. 182 and for sample No. 187 in Figure (14). Because of the brittle nature of the resin, acoustic emission was distinctly heard during testing.

The high viscosity of the BP-907 resin (8000 cps for 50% solids in ethylene dichloride) suggested that some form of diluents should be added to it. The control specimens were actually fabricated from BP-907 resin film. A dilute resin with low viscosity should ensure a more uniform penetration of the resin around all the fibers in the yarn. If improper impregnation of resin is one of the problems for a low compressive strength, then a dilute resin should increase the ultimate compressive strength. On the contrary, the stress showed a decrease as in Table XXXIX.

The effect of flexibilizing the resin was considered next. Flexibilizing the resin results in a decrease in the modulus and strength and an increase in the strain to failure. The samples were prepared by wet winding through a bath of 70% BP-907/30% Dow DER 736 flexibilized epoxy resin with 8 phr of Dow DEH 50 hardner, methylene dianiline. The resin was then diluted to 15.5 cps with ethylene dichloride. The published Dow data for this formulation using a resin similar to BP-907 lists ultimate elongation of about 8%. The average compressive strength in Table XXXIX does indicate a decrease. But the load displacement curve as in Figure (14) showed very little displacement beyond the proportional limit. An interesting observation in Figure (12) showing the failure mechanism of specimen No. 215 is the wavy nature of the fiber. However, for this exceptionally large misalignment, the compressive stress did not reflect a drastic decrease and, in addition, the nucleation of failure was at a different location where the fibers are straight.

Since the 0° - 90° Glass fabric reinforced specimen yielded a promising result, ASTM specimens were fabricated with similar properties to see whether the strength and mode of failure is altered by a change in specimen geometry. The description of these specimens, series 111B-120B, appears in Table XL. Comparison with the results for series 111-120 Table XXXIX and series 111B-120B in Table XLVI indicates no change in strength. Also, from

Figure (7), the shear band for specimen No. 115B is still in the transverse plane and not in the plane of the loading. It was also mentioned earlier in this chapter that the increase in strength for 0°-90° Glass-fabric reinforced specimens could be primarily due to the 0° Glass reinforcement. To verify this statement, specimen series 111C-120C as in Table XL was fabricated with 90° reinforcement in the form of 200 Denier PRD-49-III fibers. Results in Table XLVI suggest no significant alteration. Note the change in the load-displacement curve as compared to that for specimen nos. 115 and 125 in Figure (8). Because of the transverse reinforcement, the failure is once again in the transverse plane. This is seen from Figure (7) for specimen no. 113A which was the sandwich version of the ASTM 111C-120C series. Thus, the 0° Glass reinforcement definitely contributes to the compressive strength. However, 0° Glass reinforcement in the absence of any lateral reinforcement may not yield an ultimate strength as high as series 111-120.

The detrimental effect of 2 TPI PRD-49-III fibers was further investigated by giving a larger twist (5 TPI) to the fibers as in series 141B-150B. As indicated in Table XLVI, the decrease in strength is evident. However, because of the lack of reliable data on volume fraction, the exact decrease could not be determined.

The compression strength of the $\pm\theta°$ laminate was investigated next. The angle θ was very small (5°) so that a perturbation in the shear modulus is obtained virtually at no expense of the uniaxial strength. No increase in the ultimate value is evident in Table XLVI for this series (251-260). However, because of fiber inclination, zig-zag shear band appear as in Figure (15) with a discontinuity in the band coinciding with longitudinal splitting. The load-deformation curve for specimen no. 257 is shown in Figure (16).

Finally, failure to obtain a substantial increase in the compressive strength by alterations in the fiber interface and matrix physical and mechanical properties and by providing lateral reinforcements, led to the investigation of hybrids or blends. To this effect, sandwich specimens were fabricated from Hercules 2002 Graphite HT-S and a blend of HT-S and SP-306 as in Table XLI. Tables XLVII and XLVIII give the results for these tests. The average value for HT-S is much lower than the documented value of about 200 ksi(1.378 GN/m^2). No explanation to this discrepancy could be offered. The failure was by fiber or matrix fracture as in Figure (15). The average value of the blend was 58.8 ksi (.405 GN/m^2) and the increase is axiomatic. However, no shear band type failure was observed and the failure mode was a delamination between the HT-S and PRD-49-III layers and longitudinal splitting. The load-displacement plots for specimen nos. 263 and 275 are shown in Figure (17).

VI. SCANNING ELECTRON MICROSCOPE STUDIES

It was mentioned earlier in this report that shear or kink band formation may lead to failure of composites subjected to uniaxial compression. Kinking is a phenomenon generally associated with the crystalline structure of metals or oriented polymers and was originally observed by Orowan [32] in single crystals of Cadmium. Zaukelis [33] reported that kink bands are formed in oriented Nylon 66 and 610 by compression along the fiber axis. Seto and Tajima [34] also observed similar bands in polyethylene. Such bands can be explained by crystalline slip along the c axis (the covalent bonded chain direction). Figure (18) shows the mechanism of kinking as suggested in Reference [33]. An important observation in References [33,34] was that the kink plane is inclined to the fiber axis at an almost fixed angle which depends on the pretreatment of the fiber prior to deformation. Argon [12] suggested the formation of a failure nucleus in Boron-polyimide-epoxy fiber laminate by undergoing a process similar to kinking in metal crystals. Daniels [28] also observed a failure mode in the form of a shear band in a composite panel prepared from Hitco HMG-50 fiber. DeFerran and Harris [9] have also proposed a similar mechanism of failure for steel wire reinforced polyester resin. Since kinking, either in the plane of loading or the transverse plane was the frequent failure mode for PRD-49-III sandwich test specimens, it was decided to observe these deformations in the fiber in a scanning electron microscope. Also, PRD-49-III fiber has a highly oriented crystalline structure similar in nature to nylon and polyethylene. Graphite fiber, as manufactured from the PAN precursor, is also in a intertwinned ribbon form. For high modulus fibers, the ribbon networks tend to aling themselves in the direction of the fiber axis as is seen in Figure (19) and suggested by Diefendorf [35]. So an increase in the fiber modulus is associated with a decrease in the tensile strain and shear strength. Similarity of the crystalline structure between PRD-49-III fiber and high modulus graphite fibers, at least in the qualitative sense, explains the fact that PRD-49-III fiber is anisotropic, has a low shear modulus and a relatively poor compressive strength.

The SEM studies were conducted for sandwich specimens with the following characteristics:

1) Alumina reinforced resin;
2) 2 TPI in fiber;
3) 5 TPI in fiber;
4) 'Teflon' coated fiber;
5) 0° - 90° Glass cloth reinforcement between laminae, E-Glass fiber and HTS fiber.

In addition, PRD-49-III fiber has a high knot strength of 115 ksi (.79 GN/m^2). In view of this , it was also decided to observe the cumulative disintegration of the fiber in a SEM by progressive tying of a knot. This would enable one to observe the failure mode in tension as well as compression.

1) Alumina Reinforced Resin Specimen No. 158:

Figures (20 a,b,c,d) show different magnifications of shear band type failure observed. In Figure (20b) the presence of a slip plane in the fiber is distinctly obvious. It must be recalled here that the load-displacement curve for the Alumina reinforced resin specimen showed considerable activity in the inelastic range. This is evident from Figure (13). This may offer an explanation to the fact that there is considerable fiber damage. The salient features of Figures (20 a,b,c,d) are:

a) die marks are seen on the fiber surface; these die marks also seem to coincide with a weak diametrical plane; splitting along this plane giving rise to a 'fork' like appearance is observed in Figure (20d);

b) kinking is obvious on the fiber surface;

c) there is no evidence of bond between fiber and resin;

d) there is gross damage in the fiber and each fiber breaks up into numerous smaller diameter fibrils; this is seen in Figures (20c,d)

2) 2 TPI Fiber Specimen No. 146A:

The SEM pictures are illustrated in Figures (21 a,b,c,d). Almost similar conclusions drawn for Specimen No. 158 hold in this case. Once again, there is proof of very little interfacial bond. This is quite clear from the lower right hand corner portion in Figure (21c). Evidence of pretwisting is seen from the helical shape of the fibers. It must be noted that the PRD-49-III fiber used here is in the form of a yarn. Hence, a pretwist of 2 TPI will not be uniform in all the fibers. The break-up of individual fibers into fibrils is clearly seen in Figure (21c). Also, this disintegration seems to occur on the tension side. Figure (21d) shows partial splitting into varying sizes akin to branching from the fiber.

3) 5 TPI Fiber Specimen No. 147B:

The SEM studies performed are shown in Figures (22 a,b). In these figures, it is clearly evident that there is a complete inter-fiber splitting. The nature of bonding between the small diameter fibrils within a fiber is also visible.

4) 'Teflon' Coated Fiber Specimen No. 238:

The 'Teflon' coating was used in order to destroy the bond between the fiber and the matrix. Surprisingly, however, there is no evidence of 'Teflon' coating on the fiber surface in Figures (23 a,b). Once again splitting on a diametrical plane is noted.

5) 0° - 90° Glass Cloth Reinforcement Specimen No. 111:

As seen from Figure (7) the mode of failure for this specimen is a slip band in the transverse plane and not in the plane of loading. Accordingly, the SEM pictures in Figures (24a, b) are in the thickness direction. Figure (24b) shows the fracture of a glass fiber and also the kink band in the PRD-49-III fiber. The good matrix adhesion to the glass fiber should be noted. Figure (25a) for the E-Glass sandwich specimen no. 32 confirms the fact that the bond between the resin and E-Glass is excellent. A compressive failure in E-Glass composites involves a distinct fiber break as in Figure (4) and there is no disintegration as observed in PRD-49-III. Figure (25b) shows a higher magnification picture of Figure (25a). The compressive failure surface for HTS graphite specimen No. 267 is illustrated in Figures (26a, b). The nature of failure is similar to E-Glass and the fiber-resin bond is good. There is no evidence of inter-fiber splitting. The fiber break does not occur at an angle to the direction of loading as was suggested by Greszczuk [6]. However, a terrace type surface is obvious. That the graphite fiber consists of vertically oriented intertwinned ribbon structure is seen from a fiber in Figure (26b). But this microstructure is not very distinct as has been observed in high modulus fibers like Thornel 50S in Reference [6].

The progressive loading of a single and twin fiber knot is studied in Figures (27a,b,c,d). Figure (27b) shows the magnified view of the left end of the knot. The slip bands have just begun to appear on the compression side of the fiber. On further stretching of the knot, the bands are more distinct as in Figure (27c). In the tension side of the knot, the fiber splits into smaller diameter fibers. This is an indication of poor transverse tensile strength within the fiber. The complete splitting on the tension side is very well illustrated in Figure (27d) for a twin fiber knot.

In summary, the following conclusions can be drawn from the foregoing SEM photomicrographs:

1) There is little evidence of a good interfacial bond between the PRD-49-III fiber and resin; this is probably one of the reasons why the shear modulus and the compressive strength have a low value; an improvement in the bond should result from fiber surface treatment.

2) When subjected to compressive stress, the fiber exhibits a kink band type failure and when the strain is high, it actually splits into numerous fibrils leading to a complete loss of shear stiffness; the splitting generally occurs in the tension side; diametrically opposite die marks form a weak plane along which the fiber can split into two pieces; it must also be remembered here that the SEM photomicrographs show mainly the post failure mechanism and not the incepient failure mechanism.

VII. CONCLUDING REMARKS

Summary

Prior to the present program, studies of the compressive strength of unidirectional fiber composite materials had provided support for the hypothesis that composites containing well-collimated fiber systems, such as boron, failed due to internal instabilities. These involved fiber buckling in a fashion analogous to columns on an elastic foundation. For small diameter fibers, such as graphite, the fibers are not well collimated and it appears that local matrix and interface stresses resulting from these eccentricities contribute to compressive failure at lower stress levels. As a consequence of these facts, the present experimental study treated material changes selected to alter the fiber alignment, the lateral restraint provided to the fibers, the interface characteristics, and the matrix physical and mechanical properties. This experimental evaluation of the influence of various constituent and process characteristics upon the behavior of unidirectional PRD-49-III/Epoxy composites in compression has not resulted in any substantial increase in strength.

Theoretical evaluations carried out during this program indicate that the high degree of fiber anisotropy results in a significant drop in the predicted stress level for internal instability. This new analytical prediction of compressive strength is, however, still significantly higher than the experimental value. Treatment of partial restraint at the interface, such as that resulting from intermittent bonding or from frictional stress transfer following debonding, indicates that extremely low failure stress levels can result from this effect. However, it is not possible to assign a quantitative measure to the reduced stress transfer across a degraded interface.

Observations of the failure region with the scanning electron microscope (SEM) suggest that a high degree of interfacial debonding has occurred with the PRD-49-III fibers. Similarly, it is seen that these highly anisotropic fibers tend to fibrillate and form bundles of very small diameter fibrils. Both the internal fiber failures and the smooth surface debonding could be responsible for the measured low compressive strengths. Unfortunately the SEM observations are of post-failure phenomena. Hence, although suggestive, they are not conclusive.

Interpretation of all these results leads one to the hypothesis that PRD-49-III fiber composites under compressive loading, experience local failures within the fibers and at the interfaces. There appears to be some subsequent increase in load during which these damage sites increase in size and

number prior to overall material failure. It appears that the material changes studied experimentally during this program have influenced material behavior after the onset of damage; in some cases, to a substantial degree in terms of strain to failure.

The failure to improve compressive strength and the exposure of the fiber and interfacial failure modes, does not mean that improvement of material strength is not possible. However, the most promising approach at this stage appears to be through the use of hybrids, or blends, of two types of fibers within the composite.

Experimental Observations

Certain of the experimental measurements are directly related to the above failure hypotheses. The use of 0° - 90° glass fabric reinforcement resulted in a strength increase of about 15-20%, inhibited longitudinal splitting and changed the failure mode. However, the 90° 200 Denier PRD-49-III lateral reinforcements prevented longitudinal splitting, induced a shear band in the transverse plane but did not result in an increase in the strength. Thus, the increase in the strength of the 0° - 90° appears to be associated with the presence of glass fabric reinforcement in the 0° direction. However, the lateral reinforcement apparently permitted a significant increase in strain to failure by stabilizing the material during the damage growth stage.

Detrimental effects due to lack of fiber collimation are suggested by the comparison of boron composites with graphite composites. In the present experiments, the initial out-of-straightness of twisted yarns seem to have a degrading effect on the compression strength. However, fiber pre-stressing, intended to improve collimation, did not result in improved strength. Similarly, in specimens with extreme fiber out-of-straightness, no significant strength decrease results. Perhaps the variability of out-of-straightness from point to point in the material results in an increase in the number of damage regions which contributes to, but is not the immediate cause of, composite failure.

The use of particulate fillers resulted in increased matrix stiffness, changed matrix strength, and a decrease in fiber volume fraction. Composite strength did not improve; however, the maximum stress based on fiber area alone did show a significant increase in some cases. This increase in the compressive strength by the addition of fillers such as Alumina and Iron Oxide occurs past the proportional limit. The increase can be attributed to an improvement in the compression strength and modulus. For the Aluminum dust filled

matrix, the problem of voids and lack of surface treatment of the powder resulting in poor adhesion with the matrix resulted in a status quo of the ultimate strength based on fiber area.

Carrying this concept further, the use of moderately high modulus fibers, such as graphite, which yield higher compressive strengths, is suggested. The tests performed on a blend of PRD-49-III and HTS fibers in a unidirectional composite yielded the predicted higher compressive strength.

Recommendations

The experimental data from mechanical tests and SEM observations support the view that there are two aspects of the PRD-49-III fiber which differ greatly from observation for the graphite and glass composites. These are the existence of kink bands in the fiber and an apparent lack of evidence of adhesion of the resin on the fiber. The kink bands, a manifestation of micro-buckling of the fibrils that make up the fiber, also point out the anisotropy of the fiber. The absence of any resin particle on the fibers suggests poor adhesive strength. In either case, load transfer is expected across the interface. However, the amount of load transfer would be significantly less than complete bonding with good adhesive strength.

Both the graphite and glass specimens tested have similar geometric properties (i.e., yarns made up of many small fibers) and similar adhesive qualities with respect to the resin used. They also have similar strengths, but these compressive strengths are significantly lower than the shear-mode fiber buckling model predictions. The poor compression strength of PRD-49-III is then attributed to the inherent weakness of the fiber (as shown by the fibril micro-buckling) and to the poor adhesion qualities of this fiber. It is difficult to show prominance of one weakness over the other, i.e., to determine whether kink band formation starts first or the reduced reinforcement of the resin by its poor bond allows the fiber to deform to where it forms kink bands. The very small dimension of these fibrils suggests that the matrix is remote from the fibrils within the fiber and hence, matrix modifications may not be very promising.

The fact that so many material systems failed to perturb the compressive strength considerably suggests that the kink band formation is the inherent weakness. However, the present program did not attempt any chemical treatment designed to improve interfacial bonding. Some effort in this area appears warranted. Also, to check the effect of the structure of the fiber, the compressive strength of other members of this family of organic fibers should be investigated. The last suggestion follows from possible variations as to fibril orientation in

the fiber and its influence on the micro-buckling of kink band formation. Thus, although some graphite fibers show a fibrillar structure, they appear to have interlaced fibrils which do not experience micro-buckling at low levels. Another remedy is to investigate the effect of three dimensional reinforcements (a rather costly approach) as an improvement over the two dimensional 0° - 90° glass cloth used in this study. Finally, hybrids or blends (intimate and discrete) which utilize the low density and high tensile strength of PRD-49-III and the good compression strength of E-Glass or high strength, low modulus graphite holds promise in the immediate future.

VIII. REFERENCES

1. Moore, J.W., "PRD-49, A New Organic High Modulus Reinforcing Fiber", 27th Annual SPI Meeting, 1972.

2. Sturgeon, D.L.G., et al, "PRD-49 Fiber and Composite Performance", 17th National SAMPE Symposium, 1972.

3. Moore, J.W., et al, "Recent Advances in PRD-49 Composites", 18th National SAMPE Symposium, 1973.

4. Rosen, B.W., "Mechanics of Composite Strengthening", in Fiber Composite Materials, American Society of Metals, 1965.

5. Schuerch, H., "Prediction of Compressive Strength in Uniaxial Boron Fiber-Metal Matrix Composite Materials", AIAA J., Vol. 4, p. 102, 1966.

6. Greszczuk, L.B., "Failure Mechanics of Composites Subjected to Compressive Loading", AFML-TR-72-107.

7. Lager, J.R. and June, R.R., "Compressive Strength of Boron Epoxy Composites", J. Composite Materials, Vol. 3, p. 48, 1969.

8. Chung, W. and Testa, R.B., "The Elastic Stability of Fibers in a Composite Plate", J. Composite Materials, Vol. 3, p. 58, 1969.

9. DeFerran, E.M. and Harris, B., "Compression Strength of Polyester Resin Reinforced with Steel Wires", J. Composite Materials, Vol. 4, p. 62, 1970.

10. Greszczuk, L.B., "Microbuckling of Unidirectional Composites", AFML-TR-71-231.

11. Berg, C.A. and Salama, M., "Fatigue of Prenotched Graphite Fiber Composites in Compression", Textile Research Journal, Vol. 42, p. 222, 1972.

12. Argon, A.S., "Fracture of Composites", in Treatise of Materials Sciences and Technology, Vol. 1, Academic Press, 1972.

13. Davis, J.G., Jr. and Zender, G.W., "Compressive Behavior of Plates Fabricated from Glass Filaments and Epoxy Resin", NASA TN D 3918, 1967.

14. Davis, J.G., Jr., "Compressive Instability and Strength of Uniaxial Filament-Reinforced Epoxy Tubes", NASA TN D 5697, 1970.

15. Dow, N.F. and Gruntfest, I.J., "Determination of Most Needed Potentially Possible Improvements in Materials for Ballistic and Space Vehicles", GE-TIS 60SD389, 1960.

16. Hayashi, T., "On the Shear Instability of Structures Caused by Compressive Loads", Proceedings, XVI Japanese National Congress of Applied Mechanics, 1966.

17. Biot, M.A., "Mechanics of Incremental Deformations, Wiley, 1965.

18. Sadowsky, M.A., et al, "Buckling of Microfibers", J. Applied Mechanics , Vol. 34, p. 1011, 1967.

19. Hermann, L.R., et al, "Behavior of Compressively Loaded Reinforcing Wires", J. Composite Materials, Vol. 3, p. 212, 1967.

20. Lanir, Y. and Fung, Y.C.B., "Fiber Composite Columns Under Compression", J. Composite Materials, Vol. 6, p. 387, 1972.

21. Foye, R.L., "Compression Strength of Unidirectional Composites", Paper presented at AIAA, January 1966.

22. Leonard, R.W., "On the Shear Stiffness of Fabrics", J. Aerospace Sciences, March 1962.

23. ASTM Method D695-68T, "Compressive Properties of Rigid Plastics".

24. Structural Design Guide for Advanced Composites, AFML, Prepared by NAR, 1971.

25. Pagano, N.J. and Whitney, J.M., "Geometric Design of Composite Cylindrical Characterization Specimens", J. Composite Materials, Vol. 4, p. 360, 1970.

26. Miller, R.J., "End Plugs for External Pressure Tests of Composite Cylinders", Composite Materials: Testing and Design,ASTM STP460, p. 150, 1969.

27. Proposed Method of Test for Compressive Properties of Oriented Fiber Composites, Celanese Corporation.

28. Daniels, B.K., "A Test Method for 0° Compression of Graphite Reinforced Composites", Monsanto, Chemstrand Research Center, Durham, N.C.

29. Chamis, C.C., et al, "Criteria for Selecting Resin Matrices for Improved Composite Strength", NASA TM X-68166.

30. Dow, N.F. and Rosen, B.W., "Evaluations of Filament-Reinforced Composites for Aerospace Structural Applications", NASA CR-207, 1965.

31. Handbook of Epoxy Resins, McGraw Hill, 1967.

32. Orowan, E., "A Type of Plastic Deformation New in Metals", Nature, Vol. 149, p. 643, 1942.

33. Zaukelis, D.A., "Observation of Slip in Nylon 66 and 610 and its Interpretation in Terms of a New Model", J. Applied Physics, Vol. 33, p. 2797, 1962.

34. Seto, T. and Tajima, Y., "Observation of Kink Bands in Oriented Polyethylene", Japanese J. Applied Physics, Vol. 5, p. 534, 1966.

35. Diefendorf, R.J., "Fiber and Matrix Materials for Advanced Composites", in Composite Materials, AGARD-LS-55.

IX. TABLES AND FIGURES

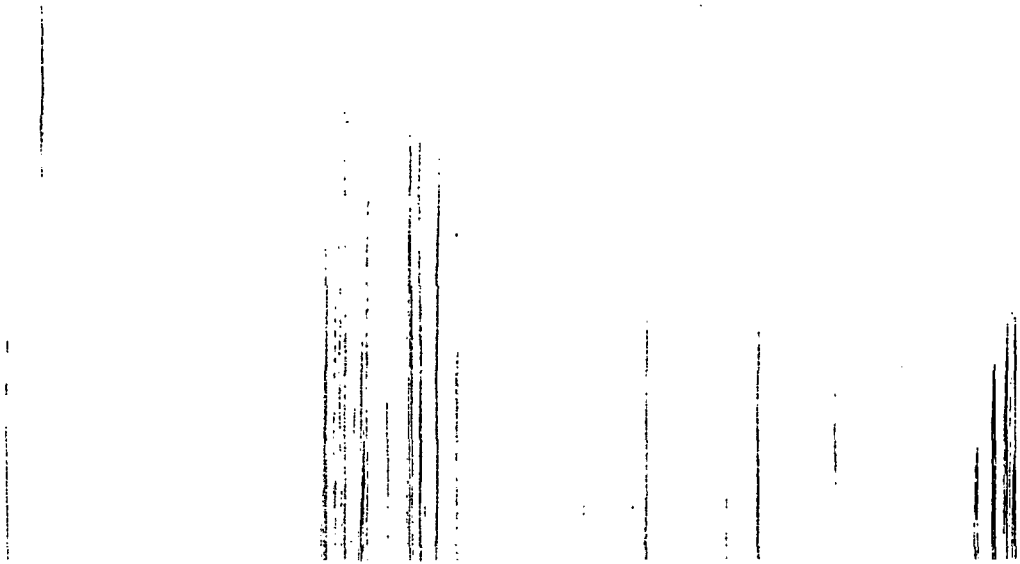

TABLE I - Properties Of PRD-49-III Fiber

Tensile Modulus	19,000 ksi (130.98 GN/m^2)
Tensile Strength based on .4 in. (10.16 cm) gage length, average of 20 breaks	580 ksi (3.99 GN/m^2)
Density	.052 pci (1.45 gm/cc)
Thermal Coefficients of Expansion	-3.6×10^{-6} in./in.,°C (Average, longitudinal) 205×10^{-6} in./in.,°C (Average, radial)

TABLE II - Properties Of PRD-49-III/Epoxy Unidirectional Laminate

Volume Fraction	.6
Longitudinal Modulus	11,000 ksi (75.83 GN/m^2)
Transverse Modulus	800 ksi (5.51 GN/m^2)
Poisson's Ratio	.34
Longitudinal Shear Modulus (Inferred from test data)	270 ksi (1.86 GN/m^2)
Ultimate Tensile Strength	180 ksi (1.24 GN/m^2)
Ultimate Compressive Strength	40 ksi (.275 GN/m^2)
Interlaminar Shear Strength	7 ksi (.048 GN/m^2)
Density	.05 pci (1.39 gm/cc)

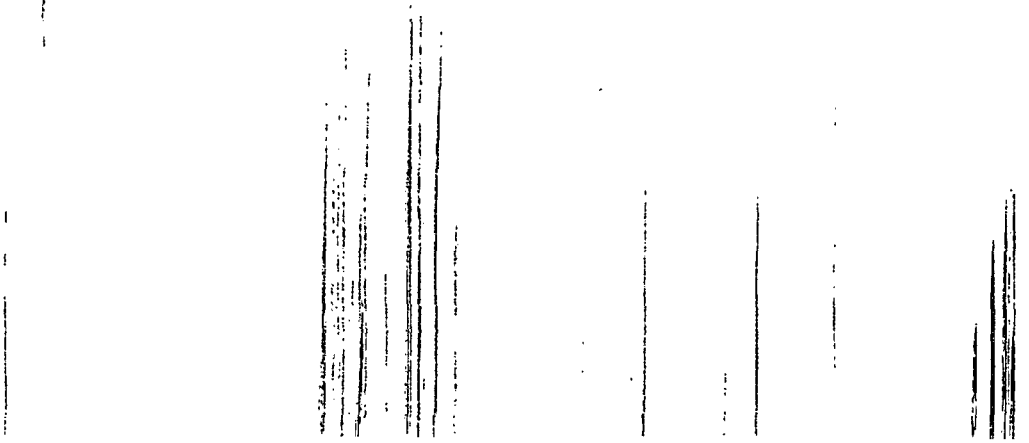

TABLE III - Description Of E-Glass Scotchply 1002 Specimens

Specimen No.	Description	Volume Fraction	Nominal Laminate Thickness in.	Nominal Laminate Thickness cm.	Nominal Width in.	Nominal Width cm.
1-10 (ASTM)	E-Glass Scotchply 1002; number of plies = 11	.49	.11	2.79	.5	12.7
1A - 10A (ASTM)	E-Glass Scotchply 1002; number of plies = 5	.49	.05	1.27	.5	12.7
11-20 (Celanese)	E-Glass Scotchply 1002 with Aluminum tabs; number of plies = 12	.48	.125	3.17	.25	6.35
21-30 (Circular Tube)	E-Glass Scotchply 1002; number of plies = 5	.51	.05	1.27	.65 (Diameter)	16.51
31-40 (Sandwich)	E-Glass Scotchply 1002; number of plies = 5	.49	.054	1.37	1.1	27.94

TABLE IV - Description Of PRD-49-III Scotchply SP-306 Specimens

41-50 (ASTM)	PRD-49-III Scotchply SP-306; number of plies = 17	.55~.6	.104	2.64	.5	12.7
41A-50A (ASTM)	PRD-49-III Scotchply SP-306; number of plies = 9	.55~.6	.055	1.39	.5	12.7
51-60 (Celanese)	PRD-49-III Scotchply SP-306; number of plies = 30	.55~.6	.175	4.44	.25	6.35
61-70 (Circular Tube)	PRD-49-III Scotchply SP-306; number of plies = 12	.55~.6	.072	1.82	.7 (Diameter)	17.78
71-80 (Sandwich)	PRD-49-III Scotchply SP-306; number of plies = 10	.55~.6	.057	1.44	.9	22.86

TABLE I - Properties Of PRD-49-III Fiber

Tensile Modulus	19,000 ksi (130.98 GN/m^2)
Tensile Strength based on .4 in. (10.16 cm) gage length, average of 20 breaks	580 ksi (3.99 GN/m^2)
Density	.052 pci (1.45 gm/cc)
Thermal Coefficients of Expansion	-3.6×10^{-6} in./in.,°C (Average, longitudinal) 205×10^{-6} in./in.,°C (Average, radial)

TABLE II - Properties Of PRD-49-III/Epoxy Unidirectional Laminate

Volume Fraction	.6
Longitudinal Modulus	11,000 ksi (75.83 GN/m^2)
Transverse Modulus	800 ksi (5.51 GN/m^2)
Poisson's Ratio	.34
Longitudinal Shear Modulus (Inferred from test data)	270 ksi (1.86 GN/m^2)
Ultimate Tensile Strength	180 ksi (1.24 GN/m^2)
Ultimate Compressive Strength	40 ksi (.275 GN/m^2)
Interlaminar Shear Strength	7 ksi (.048 GN/m^2)
Density	.05 pci (1.39 gm/cc)

TABLE V - Experimental Results For Scotchply 1002 ASTM Specimens

Specimen No.	Cross Head Speed in/min	Ultimate Compressive Stress K/in^2	GN/m^2	Modulus of Elasticity K/in^2	GN/m^2	Type of Failure
1		83.97	.5788			End delamination and longitudinal splitting
2		89.42	.6164			Same as 1
3		101.87	.7022			Same as 1
4	.015	82.35	.5677			Same as 1
5		86.11	.5936			Same as 1
6		95.05	.6552			End brooming and longitudinal splitting
7		87.27	.6016			Same as 1
	Average	89.43	.6165			

TABLE VI - Experimental Results For Scotchply 1002 ASTM Specimens

1A		95.23	.6565			End delamination and longitudinal splitting
2A		69.56	.4795			End delamination
3A	.015	86.34	.5952			Same as 1A
4A		81.95	.5649			Same as 1A
5A		97.56	.6725			Same as 1A
6A		85.10	.5866			Same as 1A
7A		58.18	.4010			Same as 1A
	Average	81.98	.5652			

TABLE VII - Experimental Results For Scotchply 1002 Celanese Specimens

Specimen No.	Cross Head Speed in/min	Ultimate Compressive Stress K/in^2	GN/m^2	Modulus of Elasticity K/in^2	GN/m^2	Type of Failure
11		91.18	.6285			Crimpled and split fibers
12		105.35	.7262			Same as 11
13		83.15	.5732			Same as 11
14*	.035	80.75	.5566	5001	34.47	Same as 11
15		107.58	.7416			Disintegration of bond between metal tab and specimen
16*		78.67	.5423			Same as 11
17		109.16	.7515			Same as 11
	Average	93.69	.6458			

TABLE VIII - Experimental Results For Scotchply 1002 Tube Specimens

21		82.27	.5671			Edge failure and longitudinal splitting
22*		93.78	.6465	4545	31.33	Same as 21
23*		66.98	.4617			Same as 21
24	.035	96.08	.6623			Column type buckling and subsequent crushing of fibers
25		93.66	.6456			Same as 21
26		91.91	.6336			Same as 21
27		72.71	.5012			Same as 21
	Average	85.34	.5883			

* - specimen with strain gages.

TABLE IX - Experimental Results For Scotchply 1002 Sandwich Specimens

Specimen No.	Cross Head Speed in/min	Ultimate Compressive Stress K/in^2	GN/m^2	Modulus of Elasticity K/in^2	GN/m^2	Type of Failure
31		83.26	.5739			Mainly fiber
32		81.24	.5600			or matrix fail-
33		81.17	.5595			ure and sub-
34		79.81	.5502			sequent separa-
35	.035	83.93	.5786			tion from core
36*		79.96	.5512			and core fail-
37*		82.49	.5686	5050	34.81	ure.
	Average	81.69	.5631			

TABLE X - Experimental Results For Scotchply SP-306 ASTM Specimens

41		34.78	.2397			Shear band
42		34.43	.2373			Shear band
43		37.13	.2559			Shear band
44	.015	34.65	.2388			Shear band
45		36.22	.2497			Shear band
46		34.07	.2348			Shear band
47		38.00	.2619			Shear band
	Average	35.61	.2454			

TABLE XI - Experimental Results For Scotchply SP-306 ASTM Specimens

41A		35.82	.2469			End delamination and longitudinal splitting
42A		33.86	.2541			Shear band
43A		32.04	.2208			Shear band
44A		35.31	.2434			Same as 41A
45A	.015	33.45	.2306			Same as 41A
46A		32.06	.2210			Shear band
47A		32.28	.2225			Shear band
	Average	33.54	.2312			

* - specimen with strain gages.

TABLE XII - Experimental Results For Scotchply SP-306 Celanese Specimens

Specimen No.	Cross Head Speed in/min	Ultimate Compressive Stress K/in^2	GN/m^2	Modulus of Elasticity K/in^2	GN/m^2	Type of Failure
51		36.88	.2542			Shear band
52		32.35	.223			Shear band and delamination
53	.015	43.93	.3028			Same as 52
54		41.22	.2841			Shear band
55*		33.83	.2332			Shear band
56		46.68	.3218			Shear band
57*		35.65	.2457	9550	65.5	Shear band
	Average	38.64	.2664			

TABLE XIII - Experimental Results For Scotchply SP-306 Tube Specimens

61		23.46	.1617			Edge failure and longitudinal splitting
62		16.43	.1132			Same as 61
63	.035	23.93	.1649			Same as 61
64		22.98	.1584			Same as 61
65*		20.00	.1378	6945	47.85	Same as 61
66*		23.92	.1649			Same as 61
	Average	21.78	.1501			

TABLE XIV - Experimental Results For Scotchply SP-306 Sandwich Specimens

71		34.00	.2343			Shear band
72		36.38	.2508			Shear band
73		36.79	.2536			Shear band
74	.015	33.90	.2337			Shear band
75*		38.05	.2623	8090	55.77	Shear band
76*		37.70	.2599			Shear band
	Average	36.13	.249			

* - specimen with strain gages.

TABLE XV - Summary Of Experimental Results For Scotchply 1002

Specimen Type	Average Compressive Strength ksi	Average Compressive Strength GN/m^2	Standard Deviation ksi	Standard Deviation GN/m^2	Remarks
ASTM	89.43	.6165	6.34	.0437	Nominal thickness = .11 in. (2.79 cm)
	81.98	.5652	12.91	.089	Nominal thickness = .05 in. (1.27 cm)
Celanese	93.69	.6458	12.4	.0854	
Tube	85.34	.5883	10.72	.0739	
Sandwich	81.69	.5631	1.46	.0100	

TABLE XVI - Summary Of Experimental Results For Scotchply SP-306

ASTM	35.61	.2454	1.4	.0096	Nominal thickness = .104 in. (2.64 cm)
	33.54	.2312	1.43	.0098	Nominal thickness = .055 in. (1.39 cm)
Celanese	38.64	.2664	4.99	.0344	
Tube	21.78	.1501	2.74	.0188	
Sandwich	36.13	.249	1.63	.0112	

TABLE XVII - Properties Of BP-907 Resin

Tensile Modulus	450 ksi (3.1 GN/m^2)
Tensile Strength	13 ksi (.089 GN/m^2)
% Elongation at Break	4.8%
Compressive Modulus	600 ksi (4.13 GN/m^2)
Compressive Strength	17.8 ksi (.122 GN/m^2)
Flexural Modulus	535 ksi (3.68 GN/m^2)
Flexural Strength	21 ksi (.144 GN/m^2)
Density	.043 pci (1.22 gm/cc)
Thermal Coefficient of Expansion	25-40 x 10^{-6} in./in. °C

TABLE XVIII - Description of PRD-49-III/Epoxy Control Specimens

Specimen No.	Description	Volume Fraction	Face Sheet Thickness in.	Face Sheet Thickness cm.	Nominal Width in.	Nominal Width cm.
101-110 (Sandwich) Control	0 twist with nominal 10 g winding tension 380 ~ 400* Denier PRD-49-III in BP-907 resin film; (cured at 350°F for 2 hrs. at 100 psi); no. of plies = 12	.585	.056	1.42	.96	24.38
101B-110B (ASTM) Control	PRD-49-III in BP-907 resin; no. of plies = 24	.63	.11 (nominal)	2.79	.5	12.7

* - nominal fiber diameter is .45 mils (.011 cm) = 1.4 Denier.

TABLE XIX - Description of PRD-49-III/Epoxy Specimens with Lateral Reinforcements

Specimen No.	Description	Volume Fraction Of PRD-49-III	Face Sheet Thickness in.	Face Sheet Thickness cm.	Nominal Width in.	Nominal Width cm.
111-120 (Sandwich)	6.6v/o Style 106 Glass fabric at 0° - 90° + 56.4 v/o SP-306 PRD-49-III; no. of Glass fabric plies =18 no. of SP-306 plies =17	.564	.058	1.47	1.0	25.4
121-130 (Sandwich)	6.6v/o Style 106 Glass fabric at ±45° + 56.4 v/o SP-306 PRD-49-III; no. of Glass fabric plies =18; no. of SP-306 plies =17	.564	.058	1.47	.97	24.63

TABLE XX - Description Of PRD-49-III/Epoxy Specimens With Alterations In Fiber Physical And Surface Characteristics

Specimen No.	Description	Volume Fraction Of PRD-49-III	Face Sheet Thickness in.	Face Sheet Thickness cm.	Nominal Width in.	Nominal Width cm.
131-140 (Sandwich)	0 twist PRD-49-III with 125g winding tension in BP-907 resin; no. of plies=12	.595	.055	1.39	.935	23.75
141-150 (Sandwich)	2 TPI (Turns per Inch) PRD-49-III in BP-907 resin; no. of plies=12	.595	.055	1.39	.98	24.89
141C-150C (ASTM)	2 TPI PRD-49-III in BP-907 resin; no. of plies=24	.635	.11 (nominal)	2.79	.5	12.7
221-230 (Sandwich)	1140 Denier PRD-49-III in BP-907 resin; no. of plies=12	.57	.056	1.42	.975	24.76
231-240 (Sandwich)	55 v/o PRD-49-III (containing 5 w/o 'Teflon')in dilute BP-907 resin; no. of plies=12	.55	.062	1.57	.975	24.76
241-250 (Sandwich)	51 v/o PRD-49-III (containing 8 w/o H_2O) in dilute BP-907 resin; no. of plies=12	.51	.062	1.57	.975	24.76

TABLE XXI - Description of PRD-49-III/Epoxy Specimens With Matrix Fillers

Specimen No.	Description	Volume Fraction Of PRD-49-III	Face Sheet Thickness in.	Face Sheet Thickness cm.	Nominal Width in.	Nominal Width cm.
151-160 (Sandwich)	PRD-49-III + 4.1 v/o $A\ell_2O_3$ in dilute BP-907 resin (16cps); 20 w/o $A\ell_2O_3$ based on resin wt.; no. of plies = 12	.46	.072	1.83	1.01	25.65
161-170 (Sandwich)	PRD-49-III + 11.0 v/o Fe_2O_3 in dilute BP-907 resin (22cps); 52 w/o Fe_2O_3 based on resin wt.; no. of plies = 12	.46	.076	1.92	1.02	25.90
201-210 (Sandwich)	PRD-49-III + 19.5 v/o $A\ell$ metal dust in dilute BP-907 resin (22.5cps); 50 w/o $A\ell$ based on resin wt.; no. of plies = 12	.37	.102	2.59	.975	24.76

TABLE XXII - Description Of PRD-49-III/Epoxy Specimens With Alterations In Resin Properties

Specimen No.	Description	Volume Fraction	Face Sheet Thickness in.	Face Sheet Thickness cm.	Nominal Width in.	Nominal Width cm.
171-180 (Sandwich)	PRD-49-III + BP-907 low temperature cured resin (250°F, 95 hrs.); no. of plies =12	.58	.057	1.44	1.00	25.4
181-190 (Sandwich)	PRD-49-III + BP-907 high temperature post cured resin (400°F, 16hrs); no. of plies =12	.58	.056	1.42	1.00	25.4
191-200 (Sandwich)	PRD-49-III + dilute BP-907 resin (16.5cps); no. of plies = 12	.61	.057	1.44	.95	24.13
211-220 (Sandwich)	PRD-49-III + flexibilized BP-907 resin (8% elongation); no. of plies = 12	.625	.057	1.44	.975	24.76

TABLE XXIII - Experimental Results For PRD-49-III/Epoxy Control Sandwich Specimens

Specimen No.	Cross Head Speed in/min	Ultimate Compressive Stress K/in^2	GN/m^2	Modulus of Elasticity K/in^2	GN/m^2	Type of Failure
104*	.02	38.78	.2673	10600	73.07	Shear band
105*		39.38	.2714	10700	73.76	Shear band
106		40.92	.2821			Shear band
107		41.44	.2856			Shear band
	Average	40.13	.2766			

TABLE XXIV - Experimental Results For PRD-49-III/Epoxy Control ASTM Specimens

101B	.02	38.93	.2683			Shear band
102B		38.99	.2687			Shear band
103B		39.09	.2694			Shear band
104B		40.18	.277			Shear band
105B		39.54	.2725			Shear band
	Average	39.34	.2712			

TABLE XXV - Experimental Results For PRD-49-III/Epoxy Sandwich Specimens With 0° - 90° Glass Cloth Reinforcement

111	.02	46.12	.3179			Shear band in transverse plane
112		43.10	.2971			Shear crimping and separation from core
113		46.12	.3179			Same as 111
114*		42.23	.2911	9900	68.25	Same as 112
115*		44.82	.3089	9680	66.73	Same as 111
	Average	44.47	.3065			

* - specimen with strain gages.

TABLE XXVI - Experimental Results For PRD-49-III/Epoxy Sandwich Specimens With +45° Glass Cloth Reinforcement

Specimen No.	Cross Head Speed in/min	Ultimate Compressive Stress K/in^2	Ultimate Compressive Stress GN/m^2	Modulus of Elasticity K/in^2	Modulus of Elasticity GN/m^2	Type of Failure
121		38.15	.2630			Shear band and longitudinal splitting
122	.02	36.87	.2541			Shear band
123		37.31	.2572			Shear band
124*		37.02	.2552	8340	57.49	Shear band
125*		38.05	.2623	10100	69.62	Shear band
	Average	37.48	.2583			

TABLE XXVII - Experimental Results For PRD-49-III/Epoxy Sandwich Specimens With 125g Winding Tension

131		37.99	.2619			Shear band
132		37.14	.256			Shear band and longitudinal splitting
133		35.97	.2479			Shear band
134*	.02	32.31	.222	9700	66.87	Shear band
135*		33.05	.2278			Shear band
136		32.86	.2265			Shear band
137		30.04	.207			Shear band
	Average	34.18	.2356			

TABLE XXVIII - Experimental Results For PRD-49-III/Epoxy ASTM Specimens With 2 TPI Yarn

141C		34.95	.2409			Shear band
142C		34.87	.2403			Shear band
143C	.02	36.36	.2506			Combined slip in the longitudinal and transverse plane
144C		36.36	.2506			Same as 143C
145C		35.45	.2443			Same as 143C
	Average	35.59	.2454			

* - specimen with strain gages.

TABLE XXIII - Experimental Results For PRD-49-III/Epoxy Control Sandwich Specimens

Specimen No.	Cross Head Speed in/min	Ultimate Compressive Stress K/in^2	Ultimate Compressive Stress GN/m^2	Modulus of Elasticity K/in^2	Modulus of Elasticity GN/m^2	Type of Failure
104*	.02	38.78	.2673	10600	73.07	Shear band
105*		39.38	.2714	10700	73.76	Shear band
106		40.92	.2821			Shear band
107		41.44	.2856			Shear band
	Average	40.13	.2766			

TABLE XXIV - Experimental Results For PRD-49-III/Epoxy Control ASTM Specimens

101B	.02	38.93	.2683			Shear band
102B		38.99	.2687			Shear band
103B		39.09	.2694			Shear band
104B		40.18	.277			Shear band
105B		39.54	.2725			Shear band
	Average	39.34	.2712			

TABLE XXV - Experimental Results For PRD-49-III/Epoxy Sandwich Specimens With 0° - 90° Glass Cloth Reinforcement

111	.02	46.12	.3179			Shear band in transverse plane
112		43.10	.2971			Shear crimping and separation from core
113		46.12	.3179			Same as 111
114*		42.23	.2911	9900	68.25	Same as 112
115*		44.82	.3089	9680	66.73	Same as 111
	Average	44.47	.3065			

* - specimen with strain gages.

TABLE XXIX - Experimental Results For PRD-49-III/Epoxy Sandwich Specimens With Al_2O_3 Filler

Specimen No.	Cross Head Speed in/min	Ultimate Compressive Stress K/in^2	Ultimate Compressive Stress GN/m^2	Modulus of Elasticity K/in^2	Modulus of Elasticity GN/m^2	Type of Failure
151*		36.23	.2495	8950	61.7	Shear band
152*		33.42	.2302			Shear bands in two planes
153		35.26	.2426			Shear band
154		34.99	.2406			Shear band
155	.02	35.40	.2412			Shear bands in two planes and longitudinal splitting
156		36.44	.2509			Shear band
157		36.44	.2509			Shear band
158		36.44	.2509			Shear band
	Average	35.57	.2447			

TABLE XXX - Experimental Results For PRD-49-III/Epoxy Sandwich Specimens With Fe_2O_3 Filler

161*		37.05	.255	1002	69.07	Shear band and longitudinal splitting
162*		39.34	.2709	9200	63.42	Same as 161
163		36.69	.2523			Shear band in transverse plane and longitudinal splitting
	.02					
164		-	-			
165		37.77	.2599			Same as 163
166		32.89	.2267			Shear bands not visible (probably because of the color of Iron Oxide); longitudinal splitting
167		37.78	.2604			Same as 161
168		38.37	.2645			Shear band
	Average	37.13	.2559			

* - specimen with strain gages.

TABLE XXXI - Experimental Results For PRD-49-III/Epoxy Sandwich Specimens With Low Temperature Cured Resin

Specimen No.	Cross Head Speed in/min	Ultimate Compressive Stress K/in^2	Ultimate Compressive Stress GN/m^2	Modulus of Elasticity K/in^2	Modulus of Elasticity GN/m^2	Type of Failure
171*		36.54	.2519	1075	74.11	Shear band
172*		34.74	.2394	9140	63.01	Shear band
173		-	-			
174	.02	33.32	.2297			End failure & shear band
175		38.76	.2672			Shear band
176		32.45	.2237			Shear band
177		32.45	.2237			Shear band
178		37.71	.2599			Shear band
	Average	35.13	.2421			

TABLE XXXII - Experimental Results For PRD-49-III/Epoxy Sandwich Specimens With High Temperature Post Cured Resin

181*		33.59	.2315	9820	67.69	Transverse shear band and considerable longitudinal splitting
182*		30.05	.2068	8840	60.94	Shear band and longitudinal splitting
183		-	-			
184	.02	31.25	.2154			Same as 181
185		-	-			
186		33.10	.2281			Shear band
187		33.10	.2281			Same as 181
188		31.31	.2158			Shear band
	Average	32.06	.221			

* - specimen with strain gages.

TABLE XXXIII - Experimental Results For PRD-49-III/Epoxy Sandwich Specimens With Dilute Resin

Specimen No.	Cross Head Speed in/min	Ultimate Compressive Stress K/in^2	Ultimate Compressive Stress GN/m^2	Modulus of Elasticity K/in^2	Modulus of Elasticity GN/m^2	Type of Failure
191*		33.56	.2313	8950	61.7	Shear band
192*		38.37	.2645	9610	66.25	Shear band
193		38.78	.2673			Shear bands in two planes
194	.02	-	-			
195		36.93	.2545			Shear band in transverse plane
196		40.16	.2768			Shear band
197		35.46	.2444			Shear band
198		34.62	.2386			Shear band
	Average	36.84	.2539			

TABLE XXXIV - Experimental Results For PRD-49-III/Epoxy Sandwich Specimens With Aℓ Metal Dust Filler

201*		24.61	.1696	5750	39.64	Transverse shear band and longitudinal splitting
202*		24.61	.1696	5750	39.64	Short length discontinuous shear bands over a wide region
203	.02	25.16	.1734			Shear band and longitudinal splitting
204		25.16	.1734			Combined transverse and in-plane shear band
205		25.28	.1742			Same as 204
206		25.28	.1742			Same as 202
207		25.28	.1747			Shear band
208		25.01	.1724			Same as 202
	Average	25.04	.1726			

* - specimen with strain gages.

TABLE XXXV - Experimental Results For PRD-49-III/Epoxy Sandwich Specimens With Flexibilized Resin

Specimen No.	Cross Head Speed in/min	Ultimate Compressive Stress K/in^2	Ultimate Compressive Stress GN/m^2	Modulus of Elasticity K/in^2	Modulus of Elasticity GN/m^2	Type of Failure
211		37.78	.2604			Complex, multi-directional shear bands because of fiber initial misalignment
212*		40.48	.2790	10350	71.35	Shear bands
213		-	-			
214	.02	-	-			
215		37.54	.2588			Shear band
216		37.54	.2588			Shear band
217		40.17	.2769			Shear band
	Average	38.70	.2667			

TABLE XXXVI - Experimental Results For PRD-49-III/Epoxy Sandwich Specimens With 1140 Denier Yarn

221*		36.17	.2493	9100	62.73	Wide and extensive region of damage associated with multiple shear bands
222*	.02	36.10	.2488	8700	59.97	Same as 221
223		-	-			
224		37.35	.2574			Same as 221
225		37.35	.2574			Same as 221
226		37.35	.2574			Same as 221
	Average	36.86	.2541			

* - specimen with strain gages.

TABLE XXXVII - Experimental Results For PRD-49-III/Epoxy Sandwich Specimens With "Teflon" Coated Yarn

Specimen No.	Cross Head Speed in/min	Ultimate Compressive Stress K/in^2	GN/m^2	Modulus of Elasticity K/in^2	GN/m^2	Type of Failure
231*		32.77	.214	10600	73.07	Shear band
232*		35.98	.248	11350	78.25	Shear band
233		–	–			
234	.02	–	–			
235		–	–			
236		38.67	.2665			Shear band and longitudinal splitting
237		37.44	.2581			Shear band and longitudinal splitting
238		33.32	.2297			Shear band
	Average	35.63	.2456			

TABLE XXXVIII - Experimental Results For PRD-49-III/Epoxy Sandwich Specimens With Moisture Coated Yarn

241*		34.08	.2349	8300	57.22	Poor bond of face sheet and core resulting in separation of core
242*		35.74	.2463	9500	65.49	Same as 241
243	.02	–	–			
244		–	–			
245		–	–			
246		33.25	.2292			Same as 241
247		35.75	.2464			Shear band
248		31.60	.2178			Same as 241
	Average	34.08	.2349			

* - specimen with strain gages.

TABLE XXXIX - Summary Of Experimental Compressive Strength Results For PRD-49-III/Epoxy Specimens

Specimen No.	Volume Fraction of PRD-49-III	Average Composite Stress		(Composite Stress/Volume Fraction) Fiber Stress of PRD-49-III	
		ksi	GN/m^2	ksi	GN/m^2
Control 101-110	.585	40.13	.2766	68.59	.4728
Control 101B-110B	.63	39.34	.2712	62.44	.4304
111-120	.564	44.47	.3065	78.84	.5434
121-130	.564	37.48	.2583	66.45	.4579
131-140	.595	34.18	.2356	57.44	.3959
141C-150C	.635	35.59	.2454	56.04	.3864
221-230	.57	36.86	.2541	64.66	.4457
231-240	.55	35.63	.2456	64.78	.4464
241-250	.51	34.08	.2349	66.82	.4605
151-160	.46	35.57	.2447	77.32	.5319
161-170	.46	37.13	.2559	80.71	.5563
201-210	.37	25.04	.1726	67.67	.4664
171-180	.58	35.13	.2421	60.56	.4174
181-190	.58	32.06	.2210	55.27	.3810
191-200	.61	36.84	.2539	60.39	.4162
211-220	.625	38.70	.2667	61.92	.4267

TABLE XL - Description Of PRD-49-III/Epoxy Specimens With Lateral Reinforcements And Initial Yarn Twist

Specimen No.	Description	Volume Fraction	Face Sheet Thickness in.	Face Sheet Thickness cm.	Nominal Width in.	Nominal Width cm.
111B-120B (ASTM)	6.7 v/o Style 106 Glass fabric at 0°-90° +54 v/o SP-306 PRD-49-III; no. of Glass fabric plies = 18; no. of SP-306 plies = 17	.54	.105 (nominal)	2.66	.5	12.7
111C-120C (ASTM)	4.3 v/o 200 Denier PRD-49-III at 90° + 55 v/o PRD-49-III in BP-907 resin; no. of plies = 24	.55	.12 (nominal)	3.04	.5	12.7
141B-150B (Sandwich)	5 TPI PRD-49-III in BP-907 resin; no. of plies = 12	.6 *	.057	1.44	.88	22.35

* - volume fraction doubtful

TABLE XLI - Description Of PRD-49-III And Graphite/Epoxy Specimens

251-260 (Sandwich)	PRD-49-III Scotchply SP-306 @ +5° ; number of plies = 10	.59	.063	1.52	.885	22.35
261-270 (Sandwich)	Hercules 2002 Graphite HT-S; no. of plies = 12	.57	.045	1.14	.887	22.52
271-280 (Sandwich)	20 v/o Hercules 2002 Graphite HT-S + 35 v/o SP-306 PRD-49-III; no. of plies = 12	.55	.07	1.77	.82	20.82

TABLE XLII - Experimental Results For PRD-49-III/Epoxy ASTM Specimens With 0°-90° Glass Cloth Reinforcement

Specimen No.	Cross Head Speed in/min	Ultimate Compressive Stress K/in^2	Ultimate Compressive Stress GN/m^2	Modulus of Elasticity K/in^2	Modulus of Elasticity GN/m^2	Type of Failure
111B	.02	41.90	.2888			End delamination
112B		42.85	.2954			End delamination
113B		40.00	.2757			End delamination
114B		41.90	.2888			Shear band in transverse plane
	Average	41.66	.2872			

TABLE XLIII - Experimental Results For PRD-49-III/Epoxy ASTM Specimens With 90° PRD-49-III Reinforcement

111C	.02	35.00	.2412			Shear band in transverse plane
112C		35.59	.2453			Same as 111C
113C		35.59	.2453			Same as 111C
114C		35.89	.2474			Same as 111C
115C		35.59	.2453			Same as 111C
	Average	35.53	.2449			

TABLE XLIV - Experimental Results For PRD-49-III/Epoxy Sandwich Specimens With 5 TPI Yarn

143B	.02	34.73	.2394			Narrow kink band
144B		38.61	.2661			Same as 143B
145B		38.00	.2619			Same as 143B
146B		38.59	.2660			Same as 143B
147B		37.45	.2581			Same as 143B
	Average	37.47	.2583			

TABLE XLV - Experimental Results For PRD-49-III/Epoxy Sandwich Specimens With Layers @ ±5°

Specimen No.	Cross Head Speed in/min	Ultimate Compressive Stress K/in^2	Ultimate Compressive Stress GN/m^2	Modulus of Elasticity K/in^2	Modulus of Elasticity GN/m^2	Type of Failure
251*		40.30	.2778	10600	73.07	Shear band with longitudinal splitting along the shear band
252*		36.76	.2532	9500	65.49	Shear band
253		40.30	.2778			Same as 251
254		41.55	.2864			Same as 251
255	.02	38.02	.2621			Same as 251
256		38.34	.2643			Shear band
257		38.02	.2621			Same as 251
	Average	39.04	.2691			

* - specimen with strain gages.

TABLE XLVI - Summary Of Experimental Compressive Strength Results For PRD-49-III/Epoxy Specimens

Specimen No.	Volume Fraction of PRD-49-III	Average Composite Stress ksi	Average Composite Stress GN/m^2	Fiber Stress (Composite Stress/Volume Fraction) of PRD-49-III ksi	Fiber Stress (Composite Stress/Volume Fraction) of PRD-49-III GN/m^2
111B-120B	.54	41.66	.2872	77.14	.5318
111C-120C	.55	35.53	.2449	64.60	.4453
141B-150B	.6*	37.47	.2583	62.45	.4305
251-260	.59	39.04	.2691	66.17	.4561

* - volume fraction doubtful

TABLE XLVII - Experimental Results For Graphite HTS/Epoxy Sandwich Specimens

Specimen No.	Cross Head Speed	Ultimate Compressive Stress		Modulus of Elasticity		Type of Failure
	in/min	K/in^2	GN/m^2	K/in^2	GN/M^2	
263		82.58	.5693			Filament or
264	.02	57.62	.3972			matrix
265		82.58	.5693			fracture
266		87.48	.603			
267		72.19	.4976			
	Average	76.49	.5273			

TABLE XLVIII - Experimental Results For PRD-49-III, HTS/Epoxy Hybrid Sandwich Specimens

271*	.02	58.00	.3998	13500	93.07	Same as 275
272*		53.79	.3709	13000	89.62	Same as 275
273						
274		64.02	.4413			End failure
275		60.98	.4752			Separation between HTS and PRD-49-III layers
276		57.22	.3944			End failure
	Average	58.80	.4053			

*specimen with strain gages.

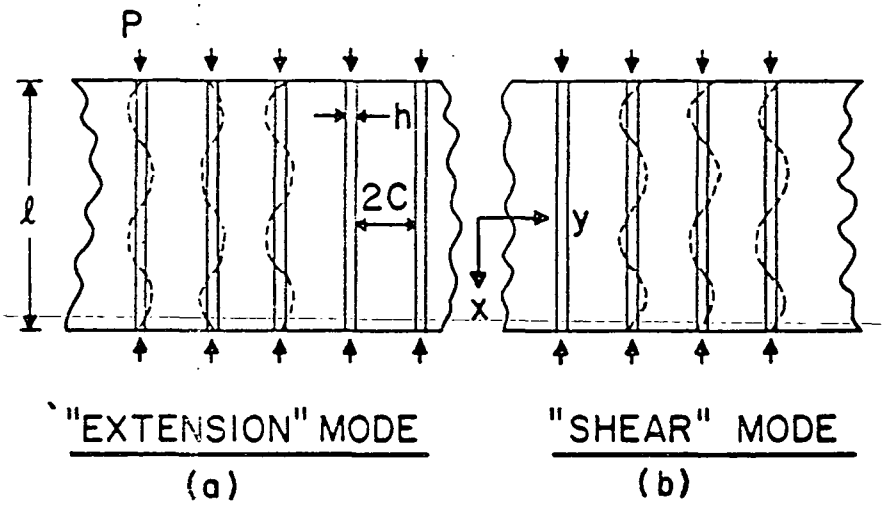

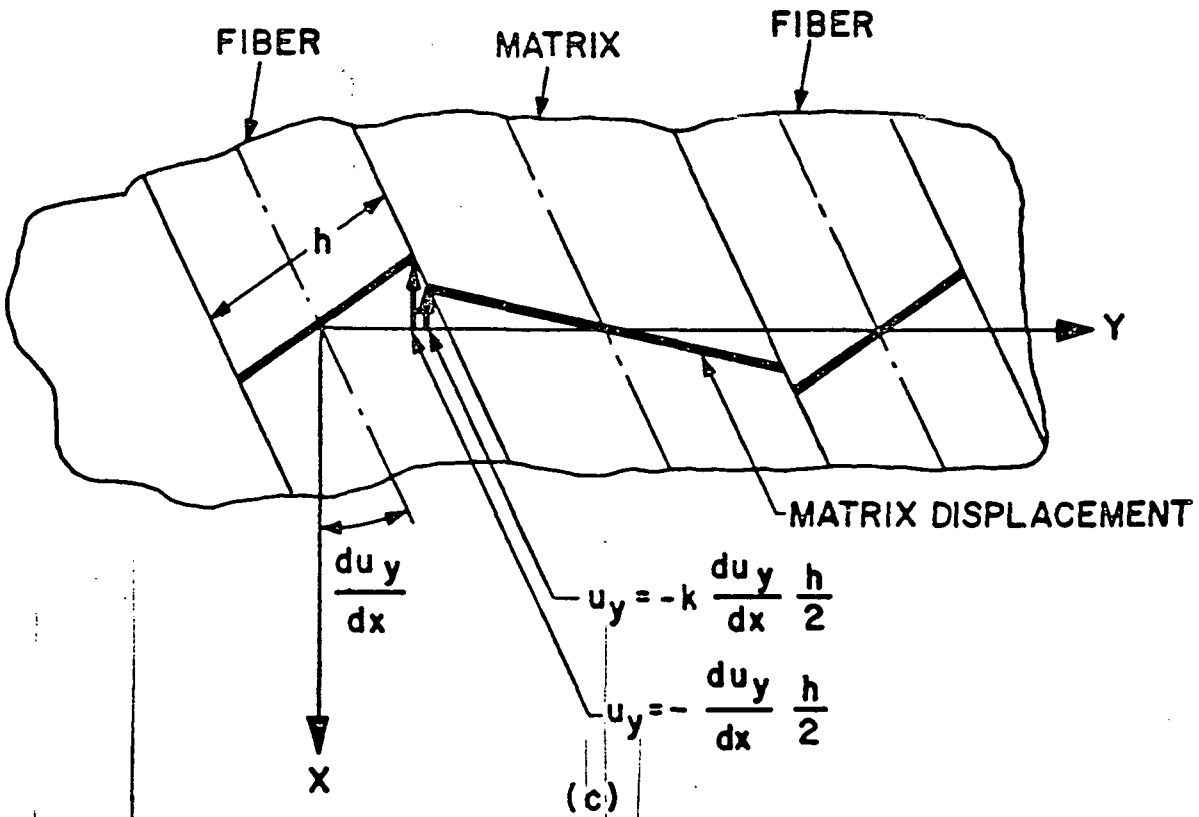

Figure (1) - Various Forms of Deformation in Fiber and Matrix

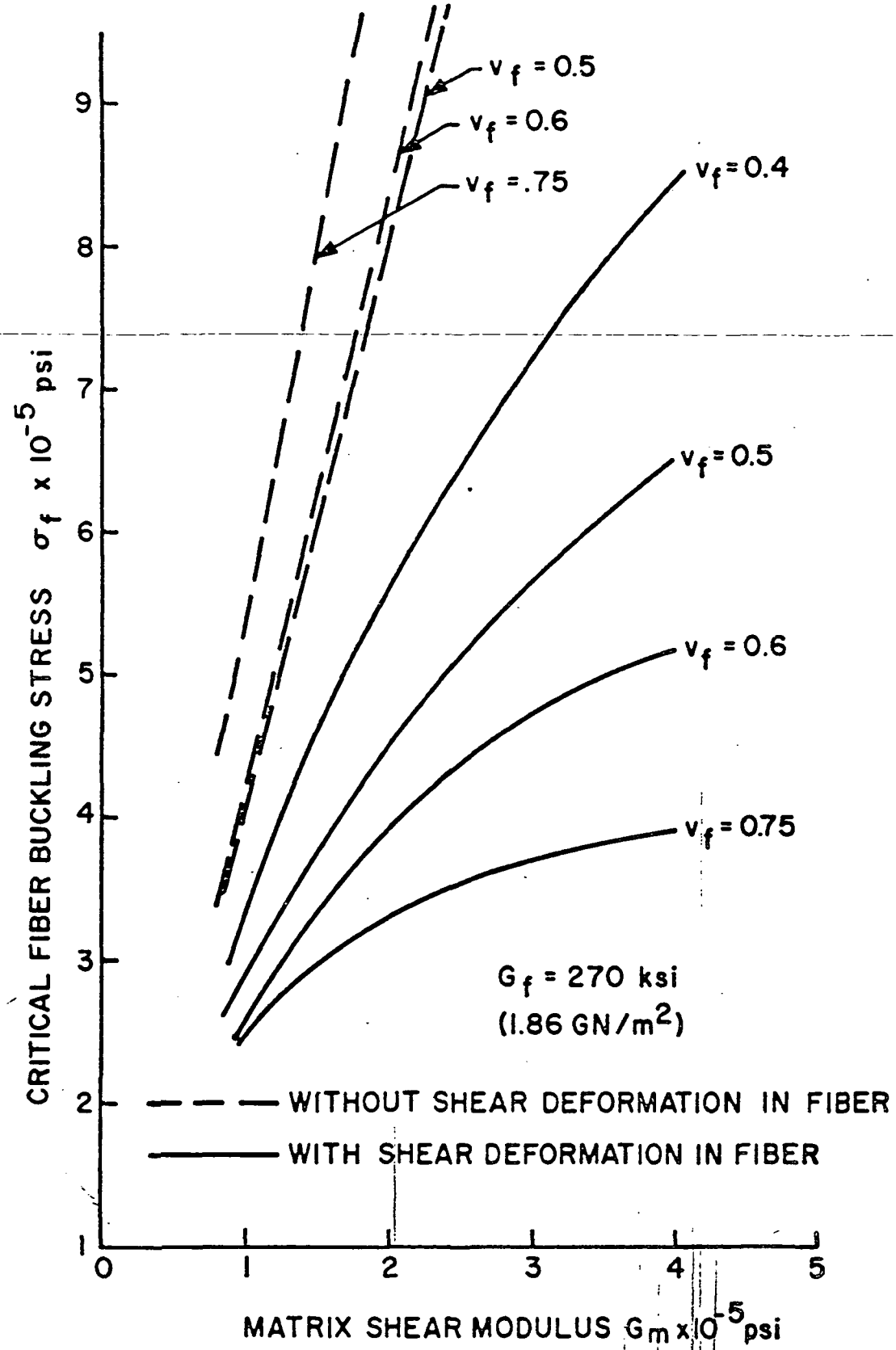

Figure (2) - Variation of Critical Fiber Buckling Stress with Matrix Shear Modulus

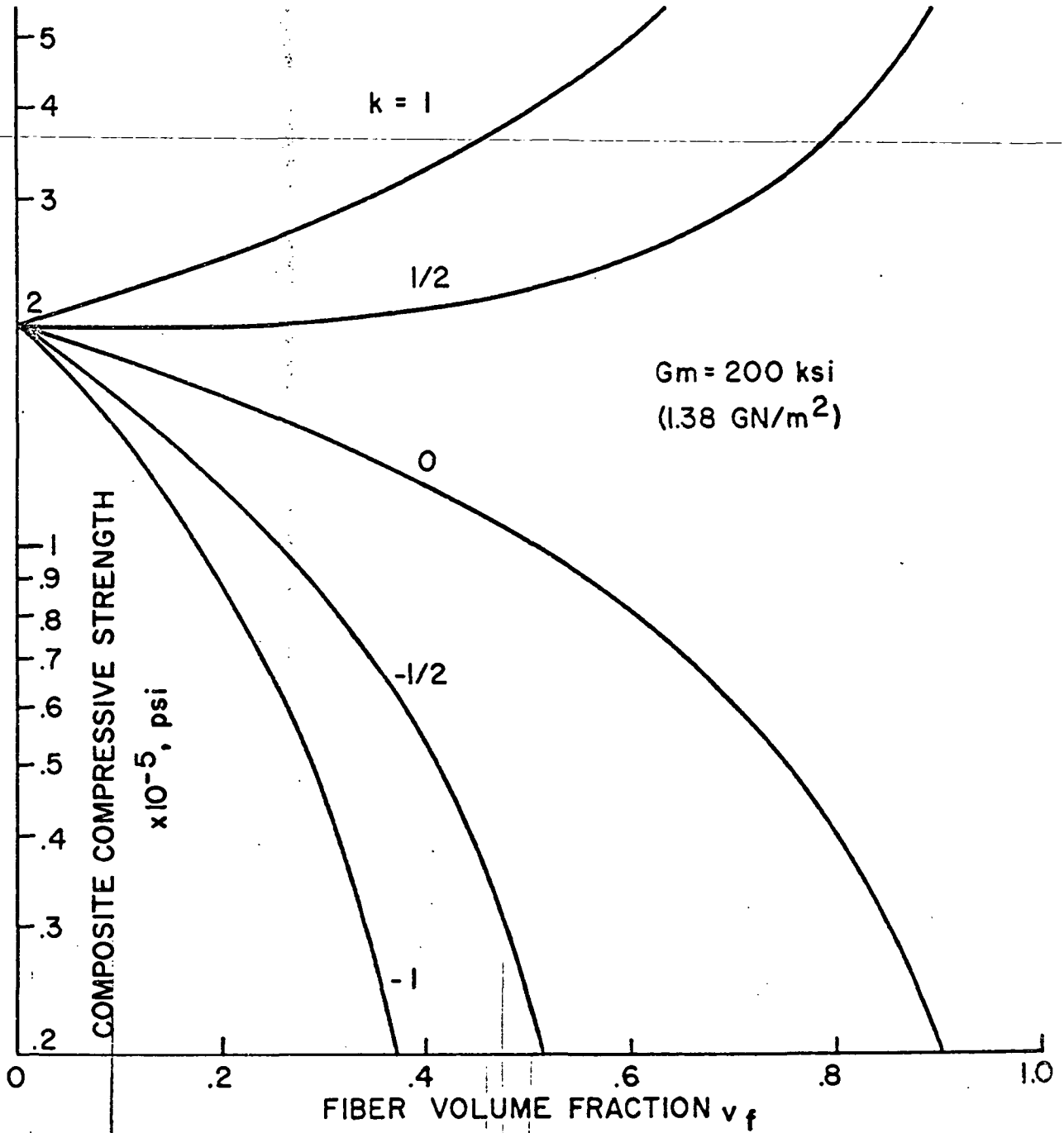

Figure (3) - Variation of Critical Composite Stress with Fiber Volume Fraction with Interfacial Slip

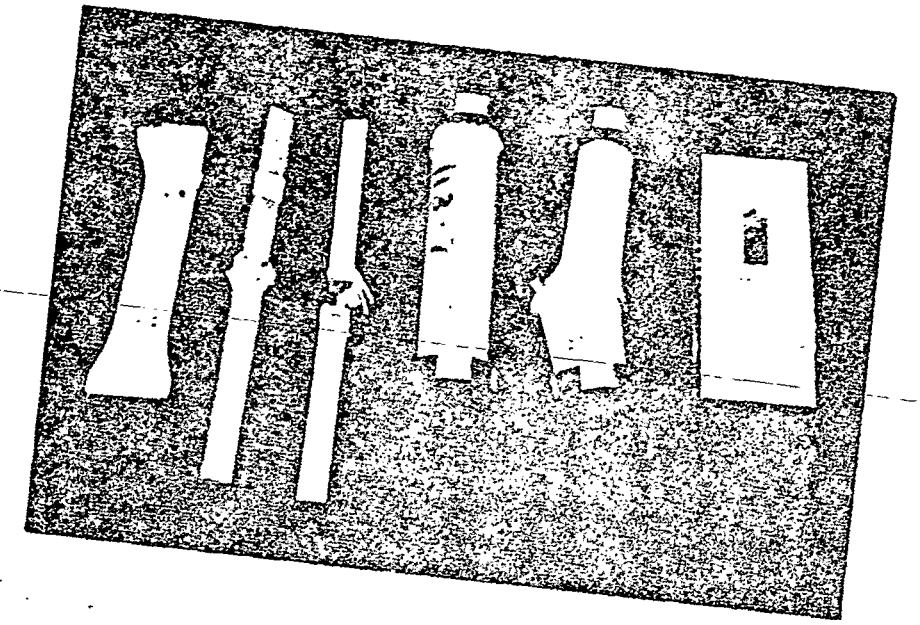

Figure (4) - Failure Modes for E-Glass Specimens

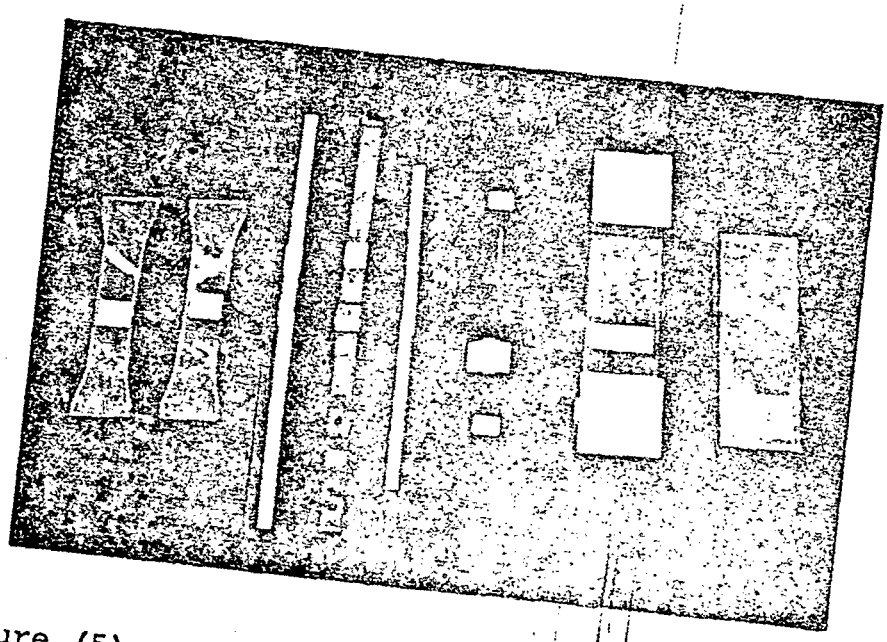

Figure (5) - Failure Modes for PRD-49-III Specimens

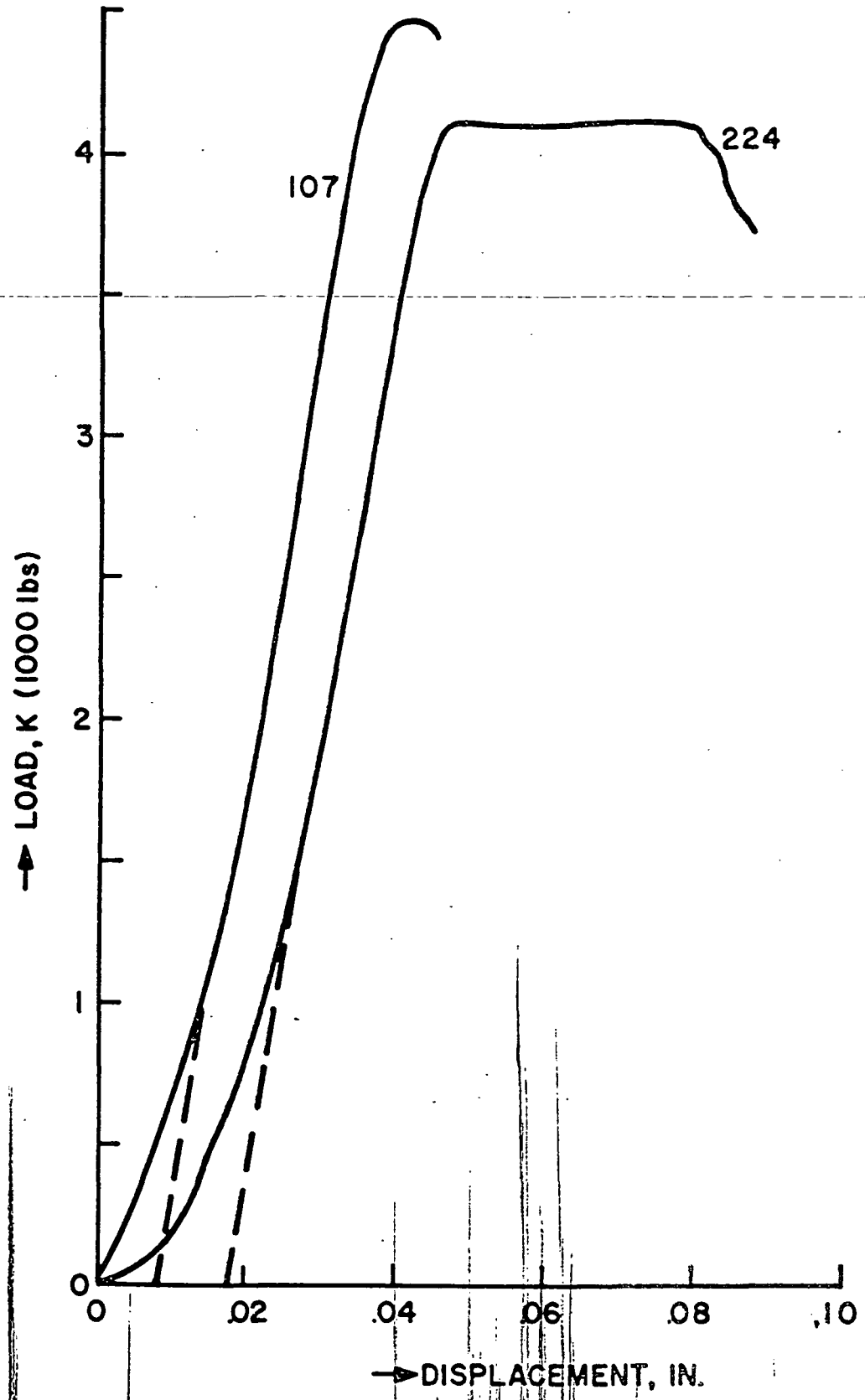

Figure (6)-Load-Deflection Curves for Control Specimen (No. 107) and 1140 Denier Yarn Specimen (No. 224)

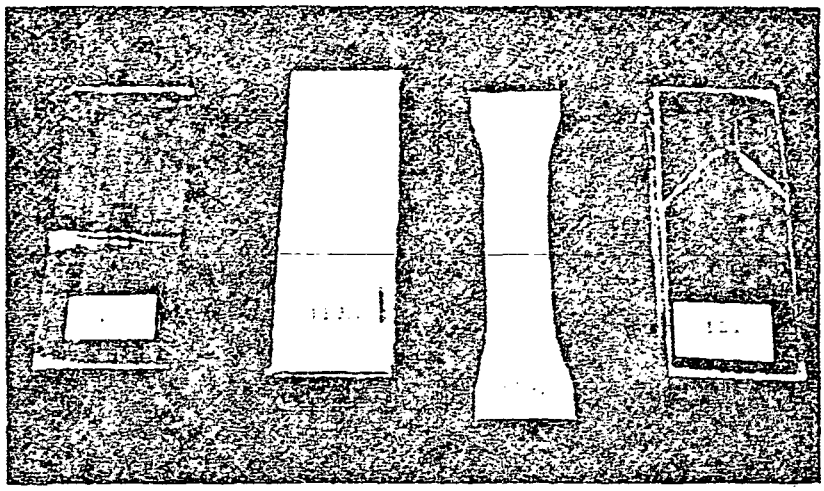

Figure (7)-Failure Modes for Speciemens with Lateral Reinforcements

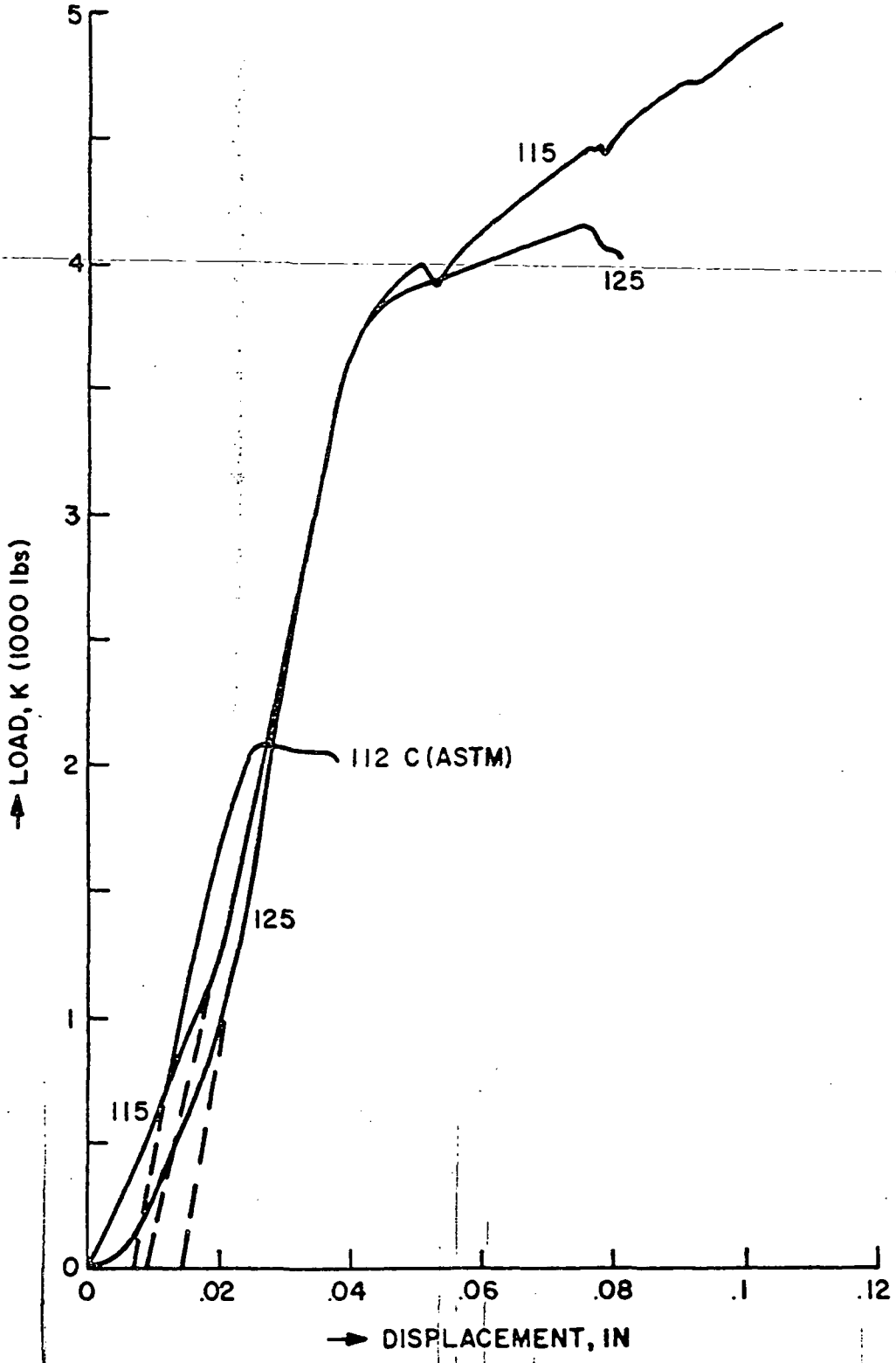

Figure (8)-Load-Deflection Curve for Specimens with Lateral Reinforcements; 0°-90° Glass Cloth (No. 115), ±45° Glass Cloth (No. 125) and 90° PRD-49-III (No. 112C)

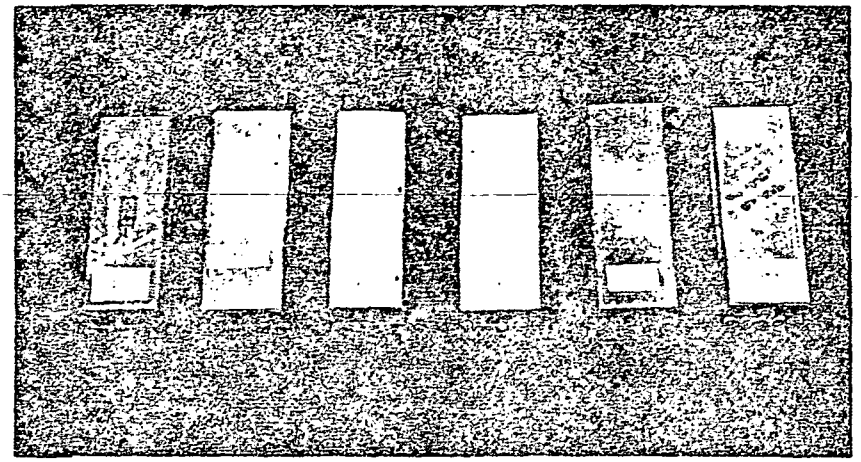

Figure (9)- Failure Modes for Various Alterations in Fiber Physical Properties

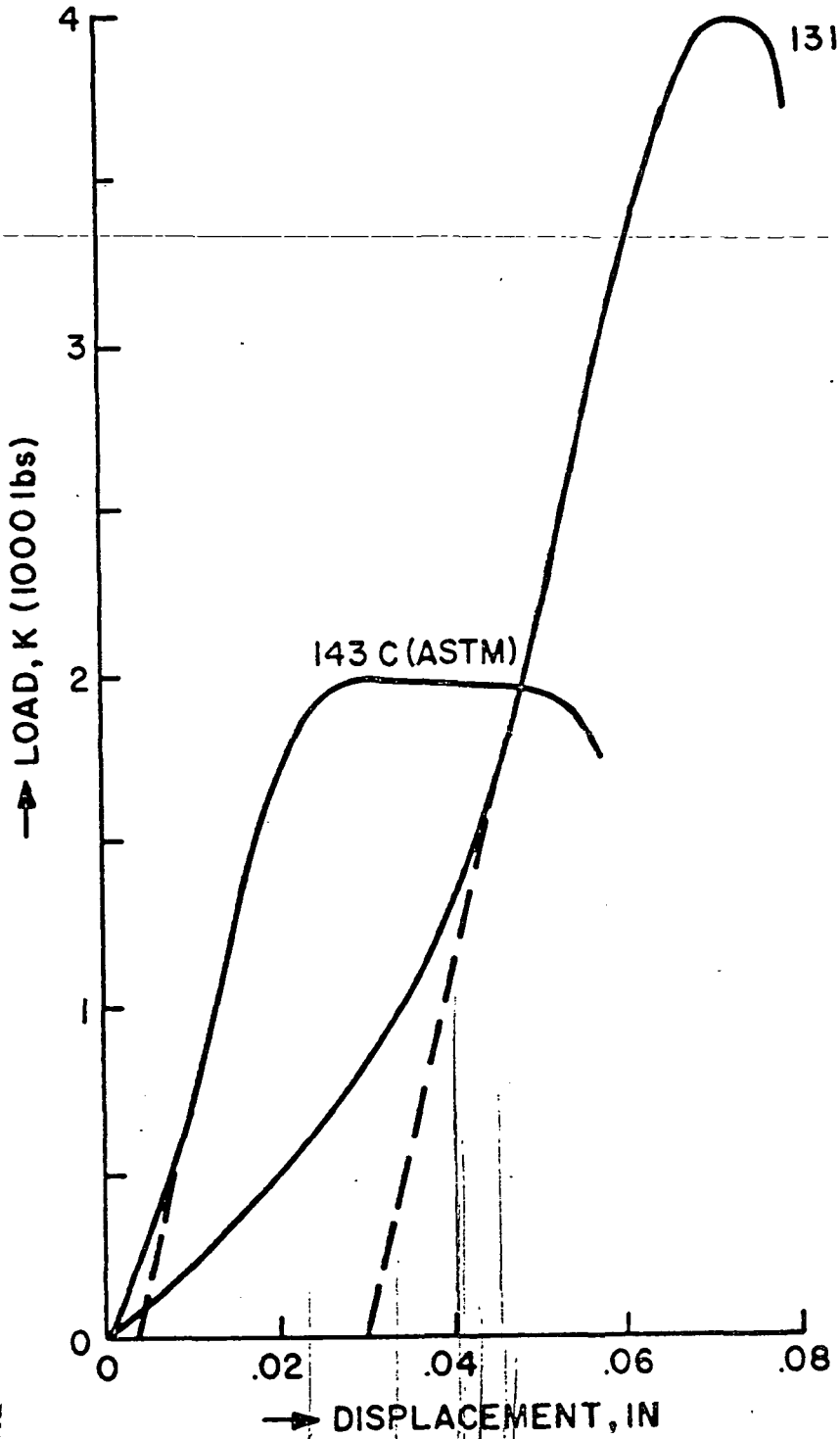

Figure (10)-Load-Displacement Curves for Specimens with Initial 125g Tension (No. 131) and with Initial 2 TRI Twist (No. 143C)

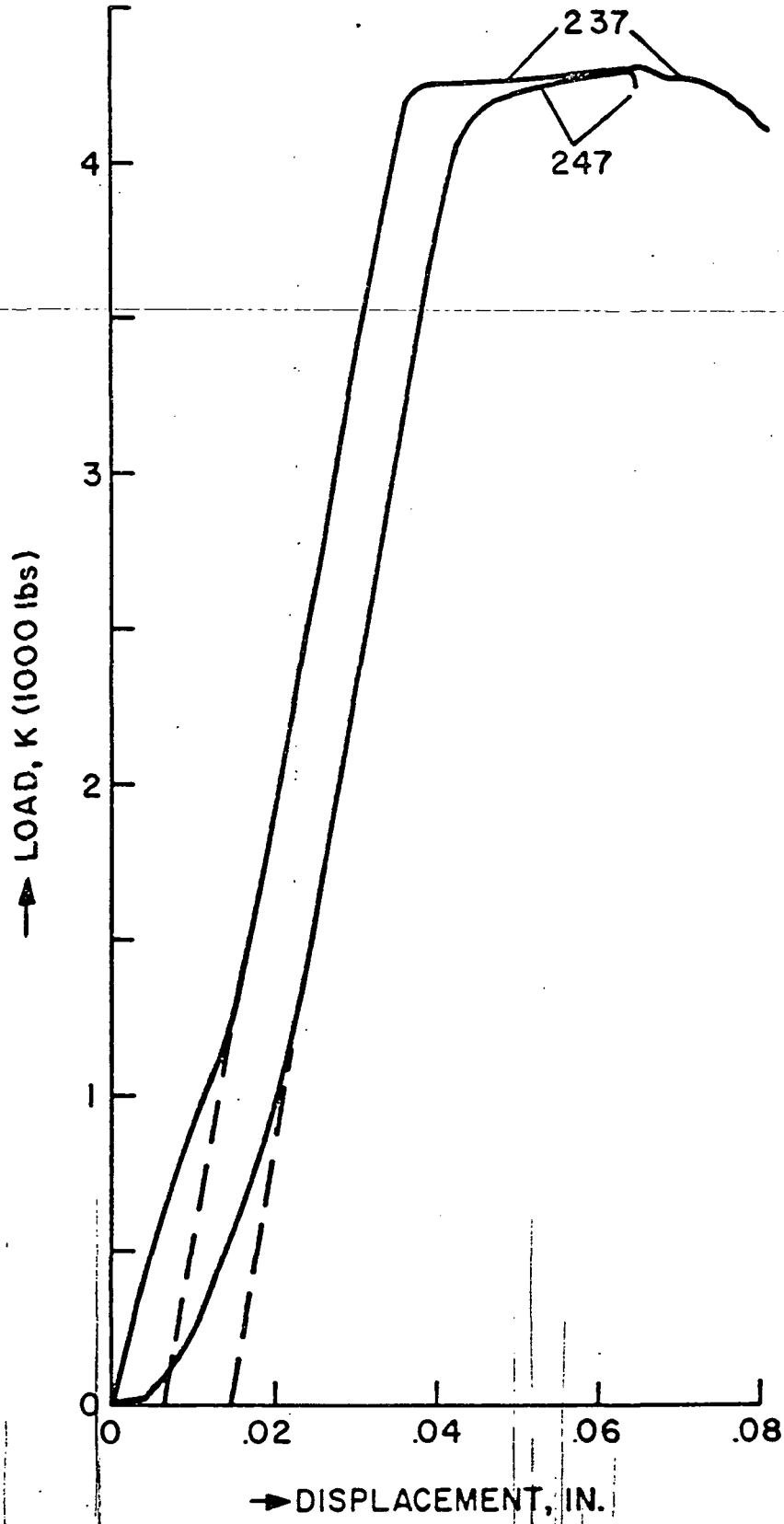

Figure (11)-Load-Displacement Curves for Specimens with 'Teflon' Coating (No. 237) and with Moisture Coating (No. 247)

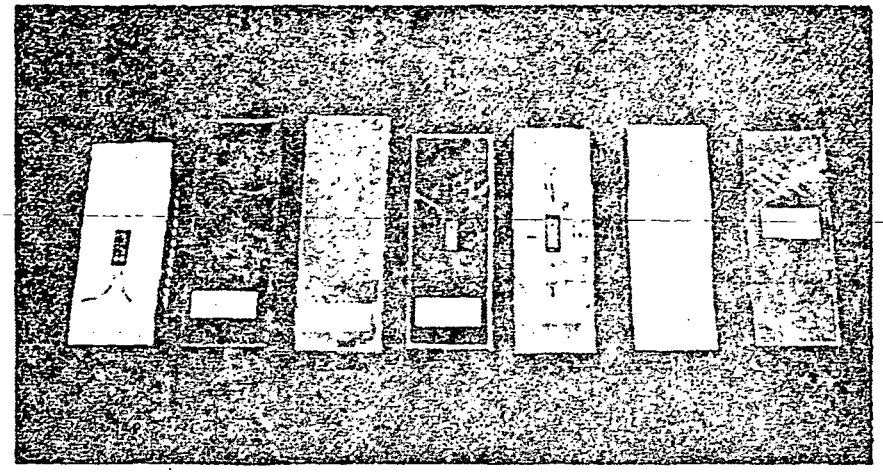

Figure (12)-Failures Modes for Various Alterations in the Physical and Mechanical Properties of the Matrix

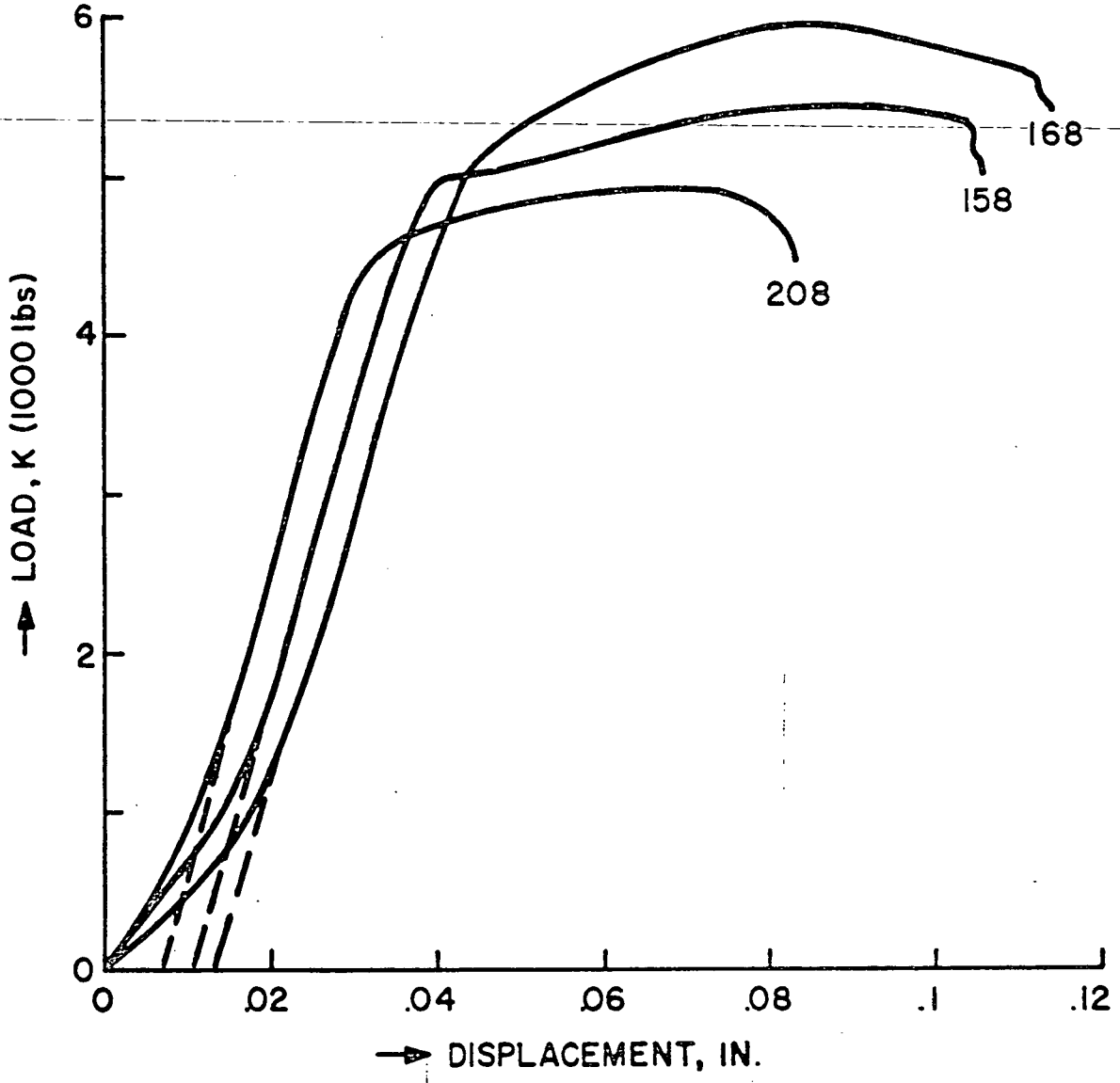

Figure (13)-Load-Deflection Curves for Specimens with Fillers; Alumina (No. 158), Iron Oxide (No. 168) and Aluminum Metal Dust (No. 208)

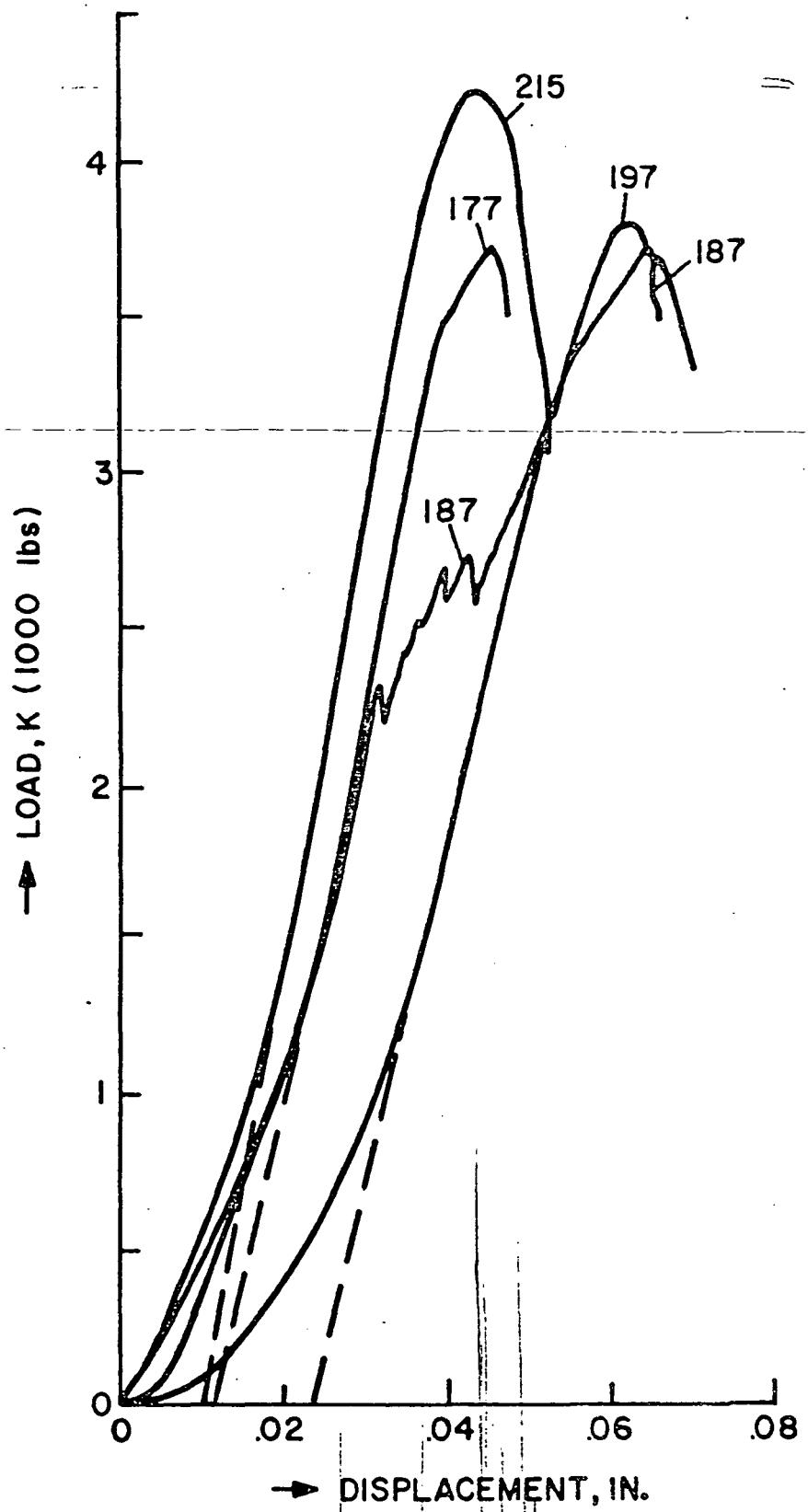

Figure (14)-Load-Deflection Curves for Specimens with Various Alterations in Matrix Properties; Low Temperature Cured (No. 177), High Temperature Post Cured (No. 187), Dilute Resin (No. 197) and Flexibilized Resin (No. 215)

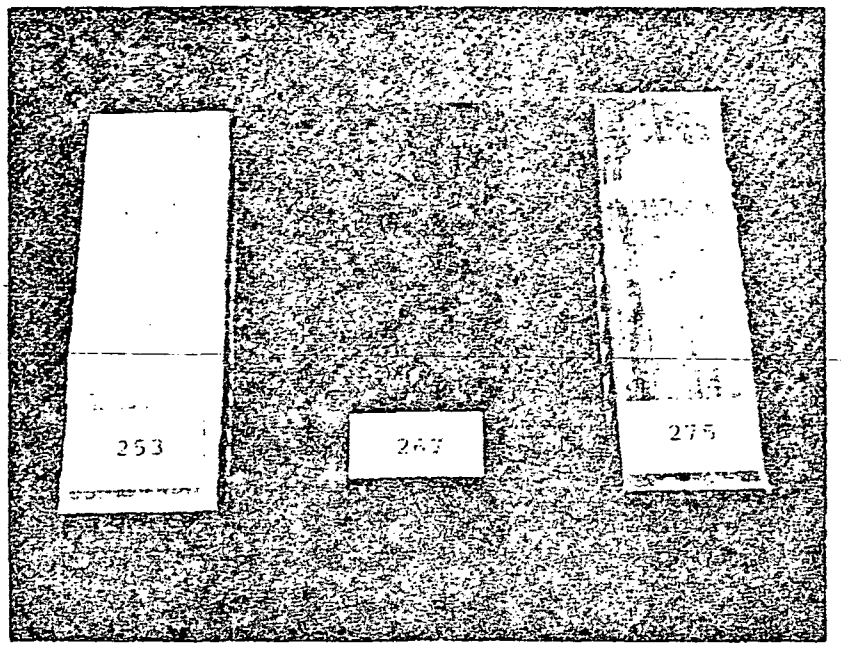

Figure (15)-Failure Modes for ±5° Orientation PRD-49-III (No. 253), HT-S Graphite (No. 267) and HT-S /PRD-49-III Blend (No. 275)

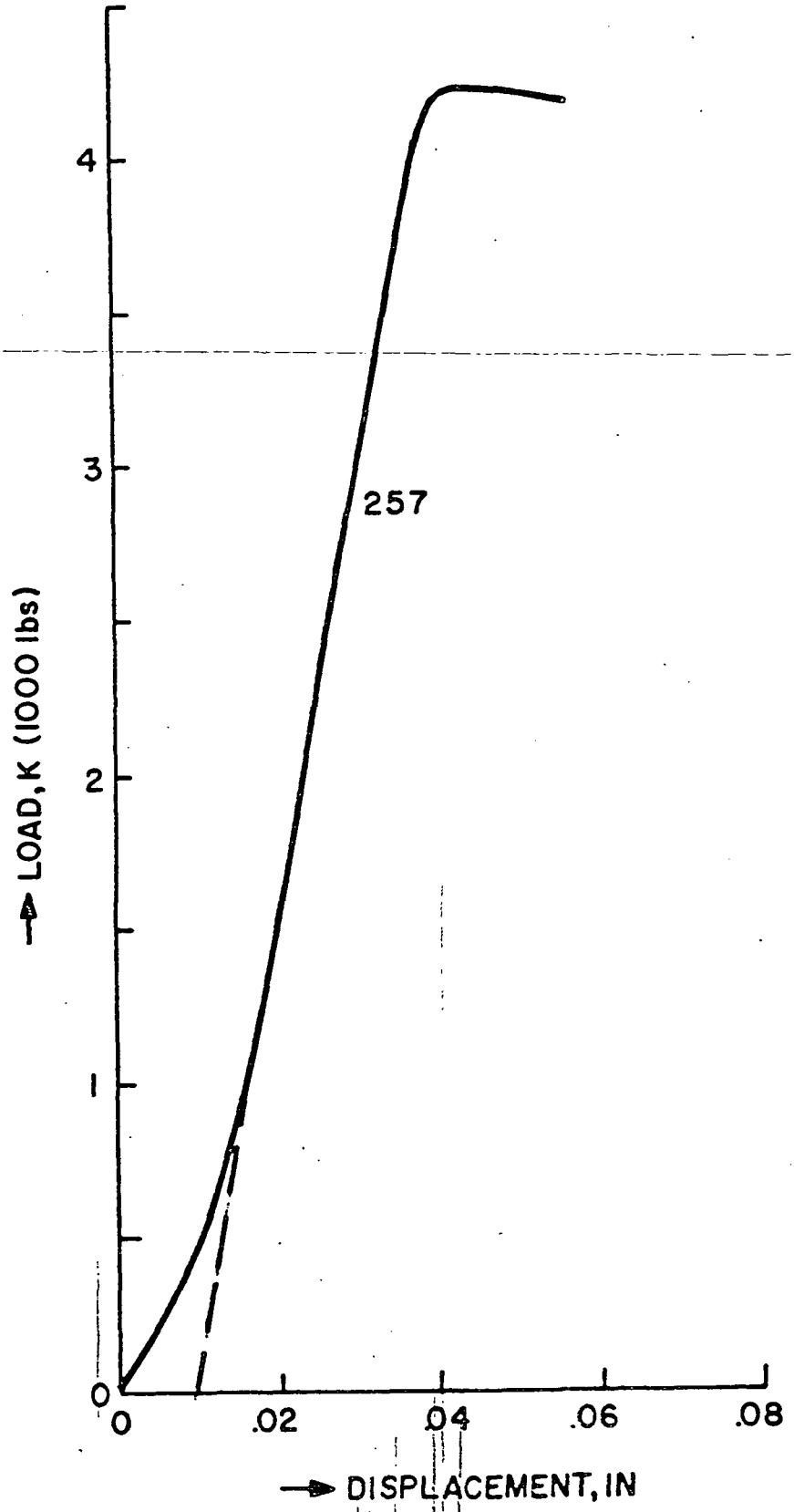

Figure (16)-Load-Displacement Curve for ±5° Orientation
PRD-49-III

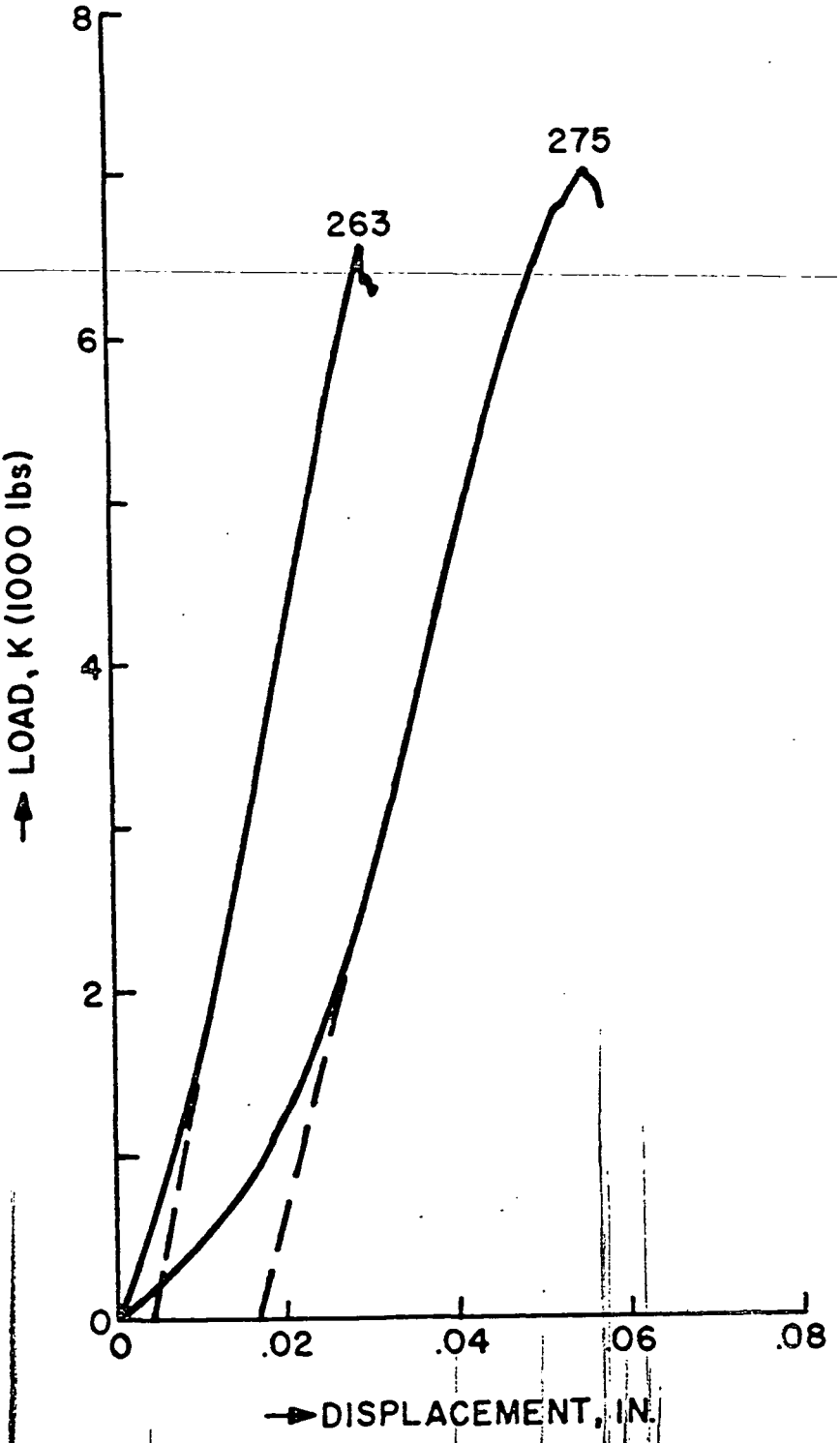

Figure (17)-Load-Deflection Curves for HT-S Graphite (No. 263) and HT-S/PRD-49-III Hybrid (No. 275)

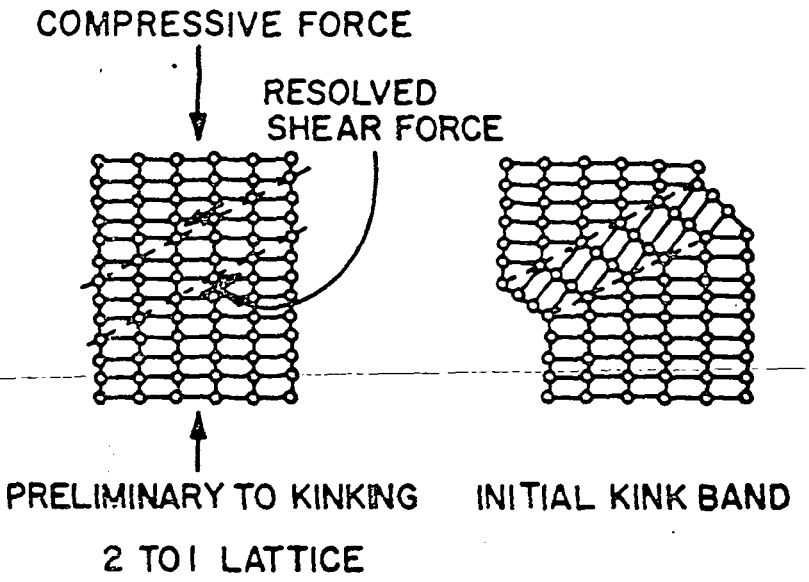

Figure (18)-Kink Band Formation Mechanism as Suggested in Reference [36]

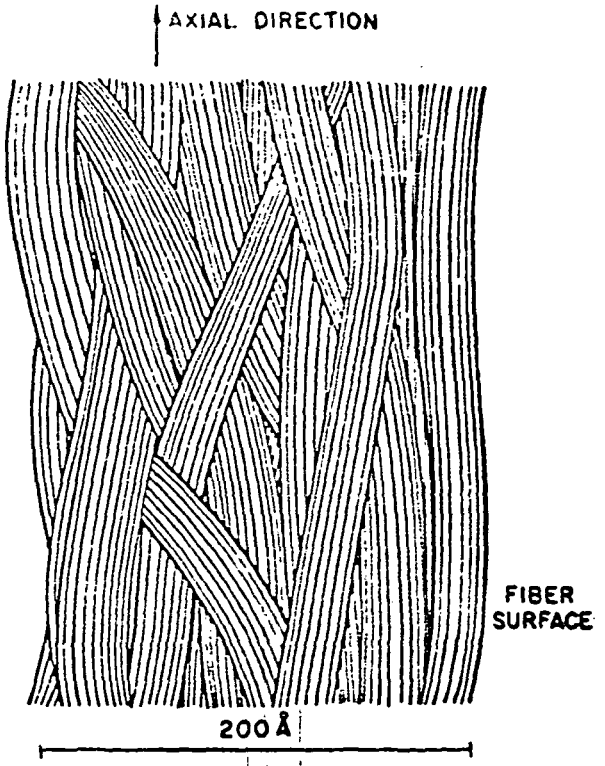

Figure (19)-Ribbon Structure of Graphite Fiber From Reference [38]

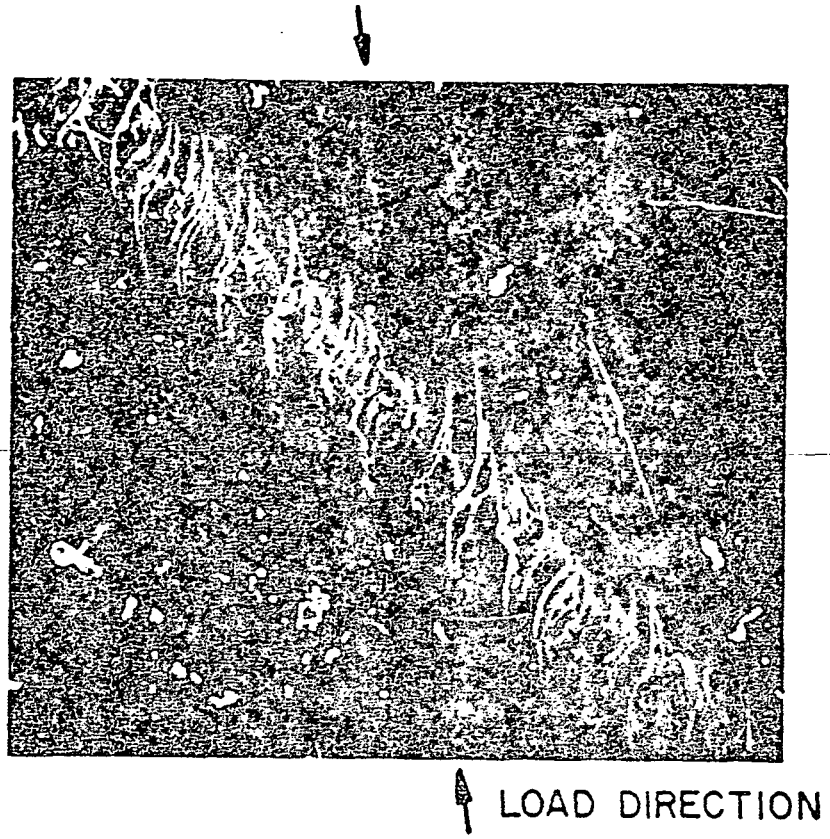

Figure (20a)-SEM Photomicrograph Showing Kink Band for Alumina Reinforced Matrix Specimen No. 158, x 50

Figure (20b)-SEM Photomicrograph Showing Die Yarks and Slip Planes in a Fiber in Specimen No. 158, x 1000

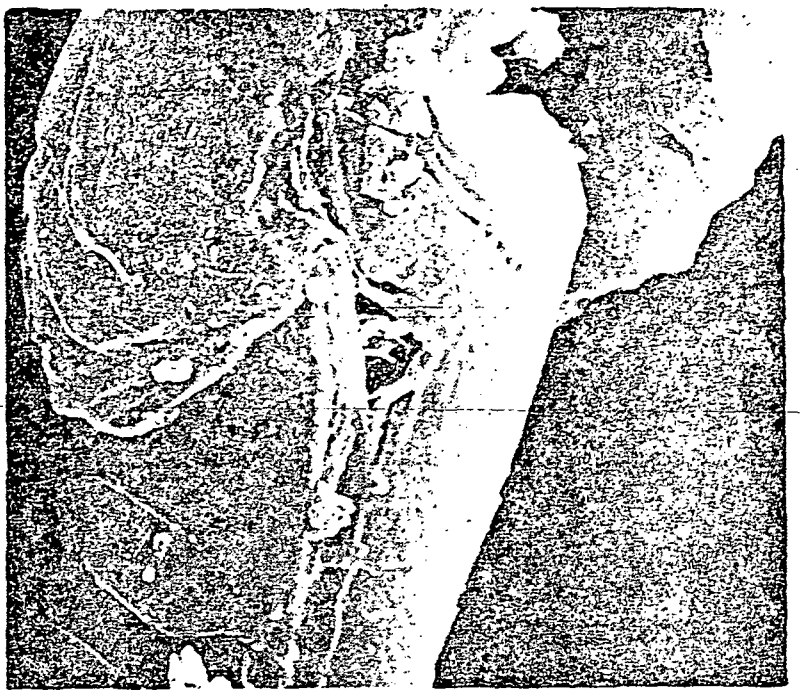

Figure (20c)-Magnified View of Figure (20b), x 3000

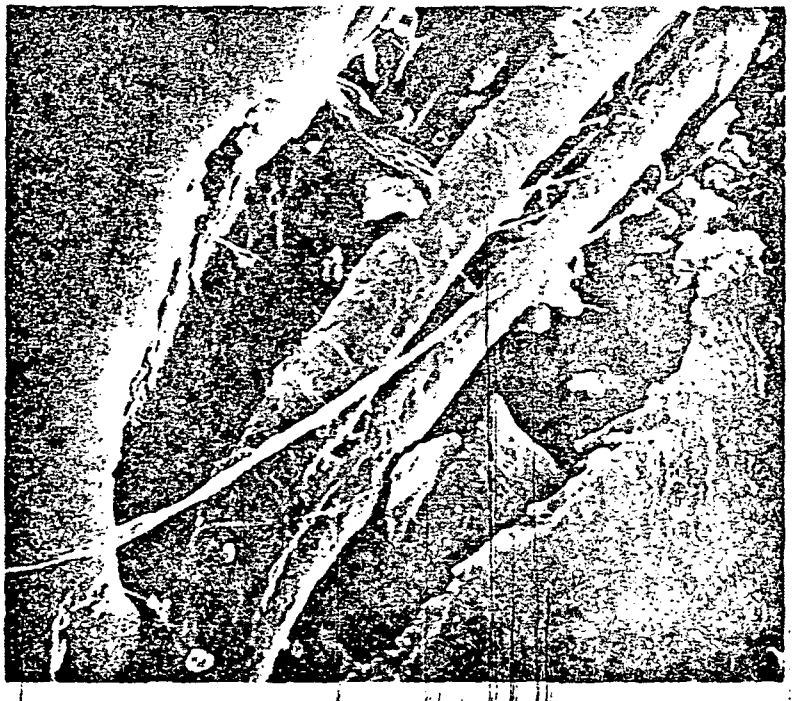

Figure (20d)-SEM Photomicrograph Showing Splitting of Fiber Along Diameterical Plane for Specimen No. 158, x 1000

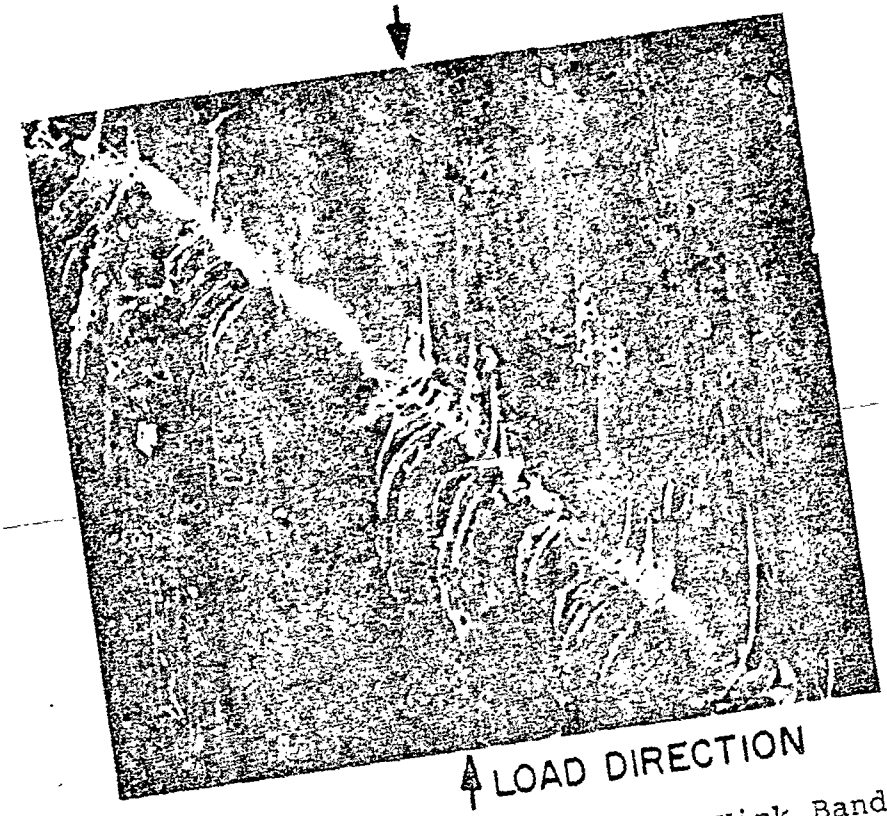

Figure (21a)-SEM Photomicrograph of Kink Band in 2 TPI Specimen No. 146A, x 50

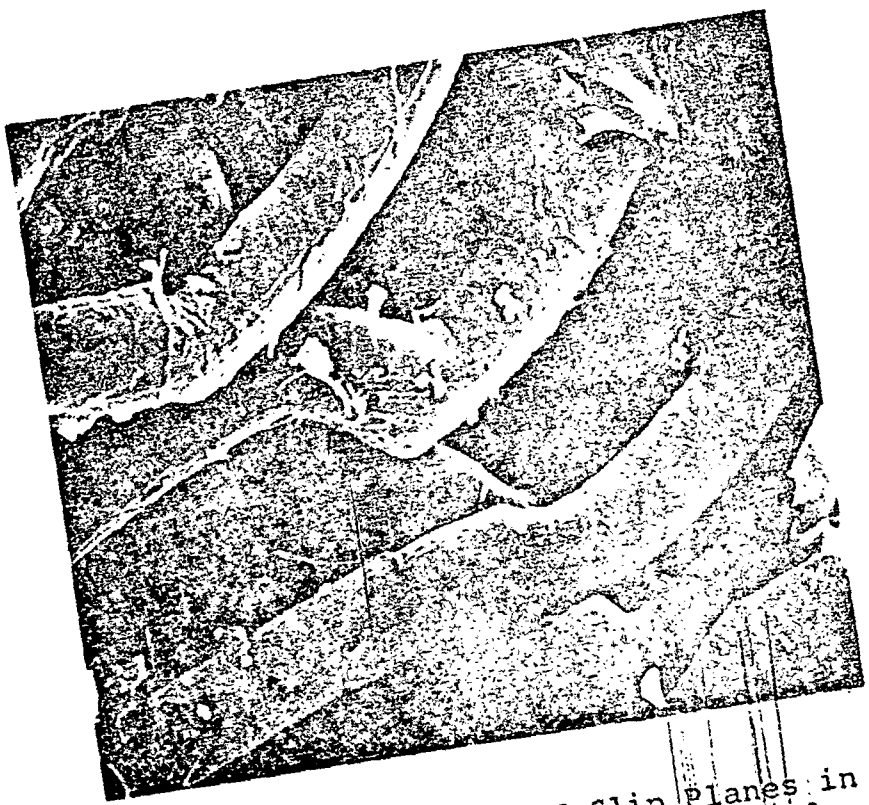

Figure (21b)-SEM Photomicrograph of Slip Planes in Individual Fibers in Specimen No. 146A, x 1000

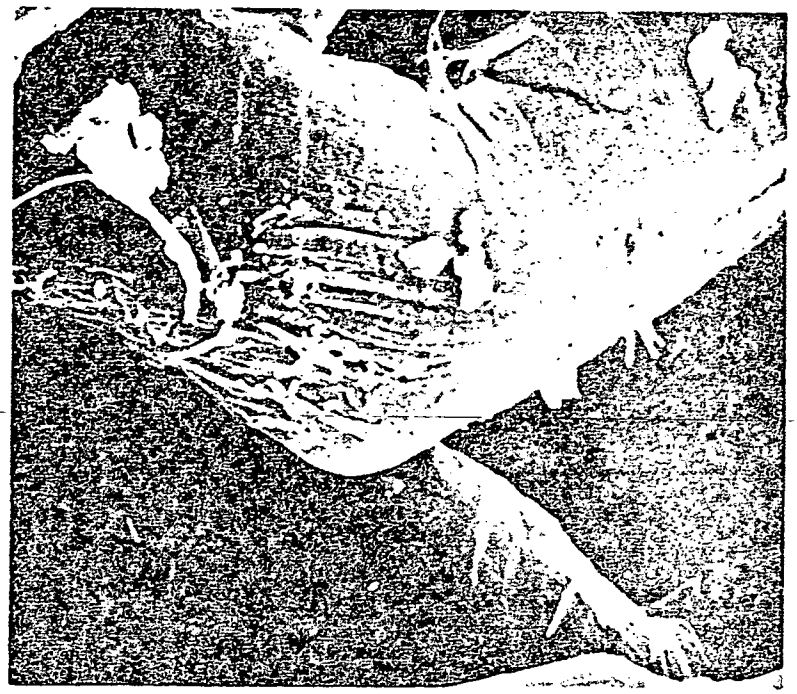

Figure (21c)-Magnified View of Figure (21b), x 3000

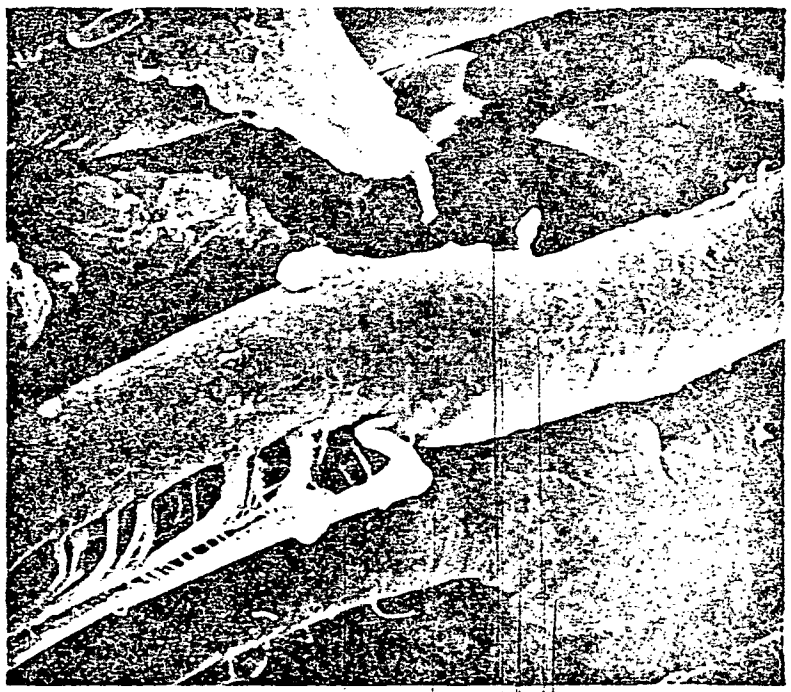

Figure (21d)-SEM Photomicrograph Indicating Partial Fiber Splitting or Branching in Specimen No. 146A, x 1500

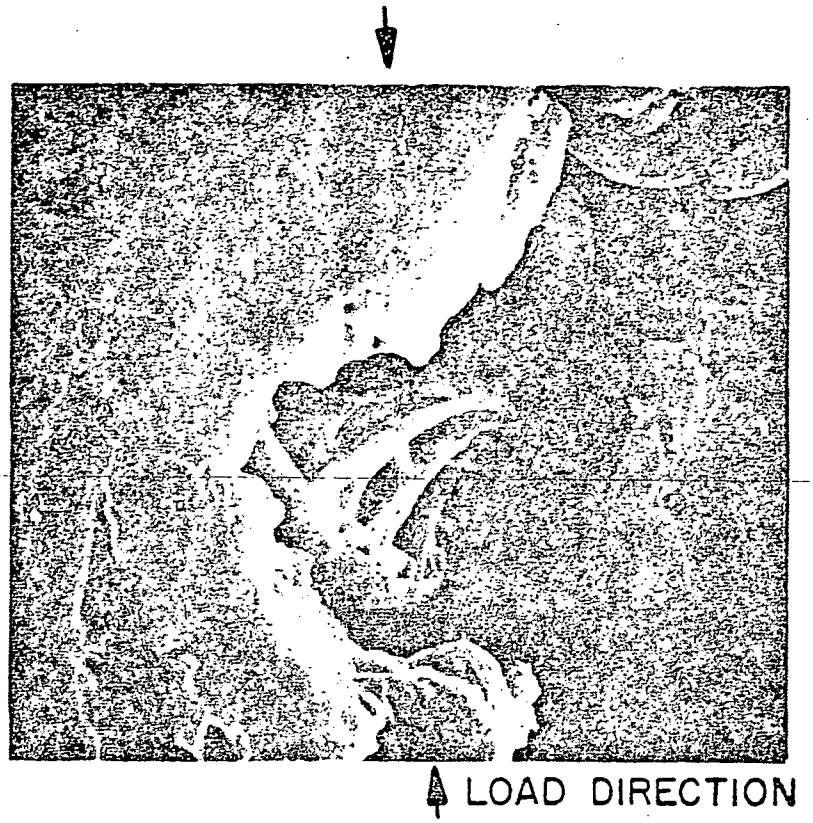

Figure (22a)-SEM Photomicrograph Showing Complete Fiber Disintegration in 5 TPI Specimen No. 147B, x 1000

Figure (22b)-Magnified View of Figure (22a), x 3000

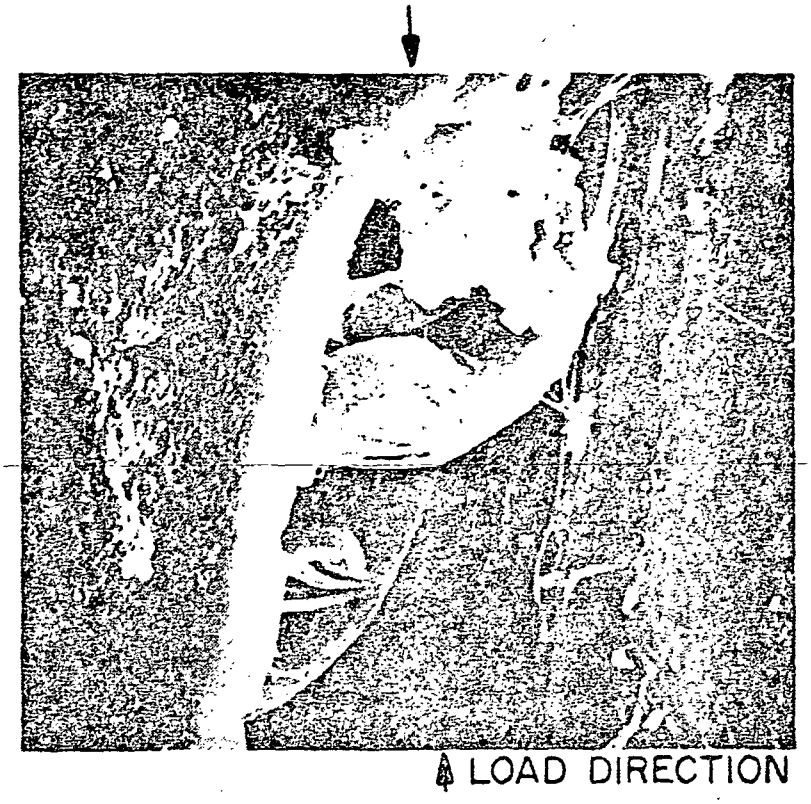

Figure (23a)-SEM Photomicrograph Showing Fiber Splitting Apart in 'Teflon' Coated Specimen No. 238 and Absence of 'Teflon' Coating on Fiber, x 1000

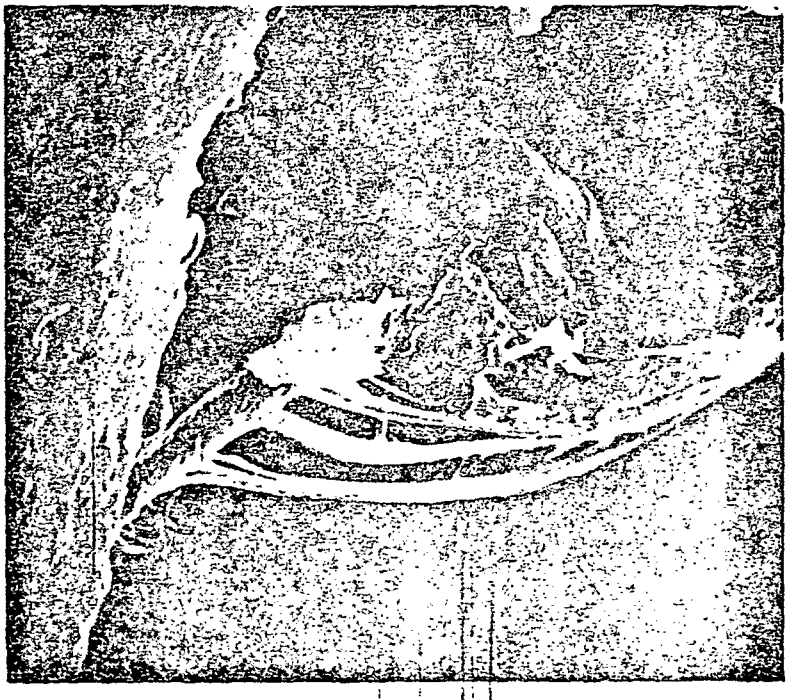

Figure (23b)-Magnified View of Figure (23a), x 3000

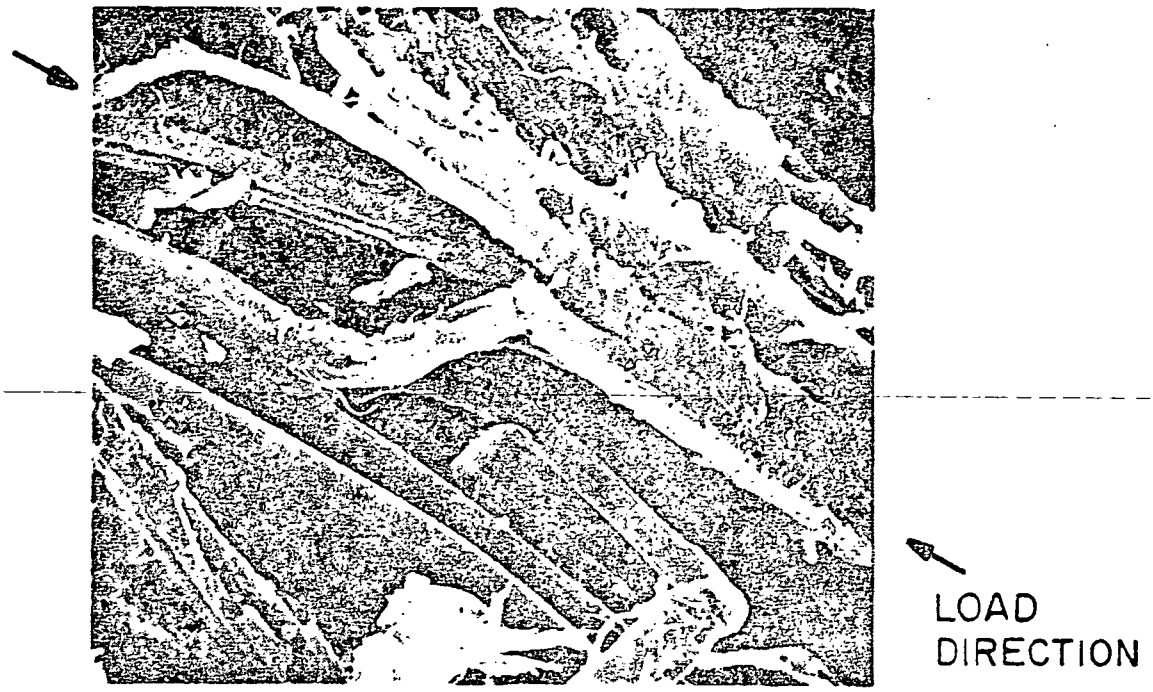

Figure (24a)-SEM Photomicrograph Showing Glass and PRD-49-III Fiber Failures in 0°-90° Glass Reinforced Specimen No. 111, x 300

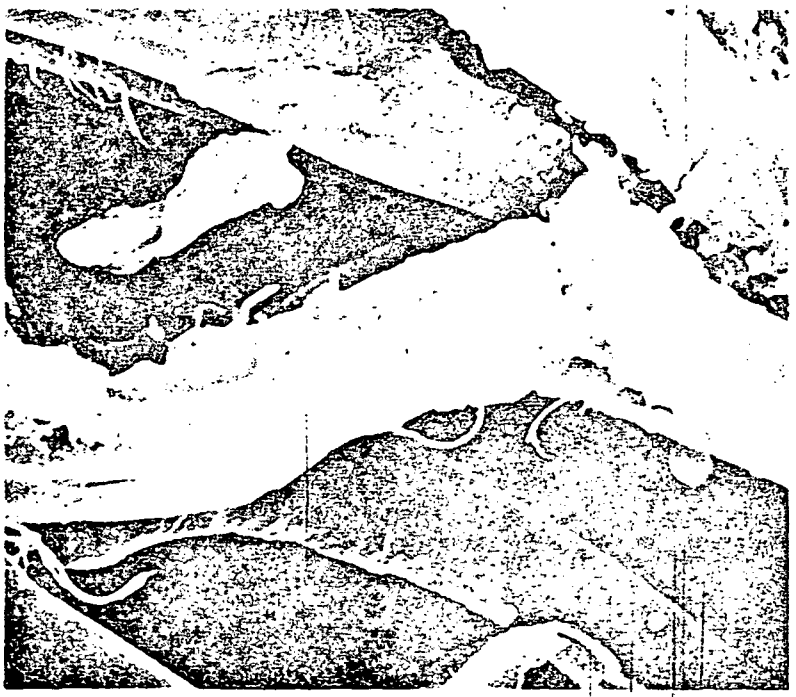

Figure (24b)-Magnified View of Figure (24a), x 1000

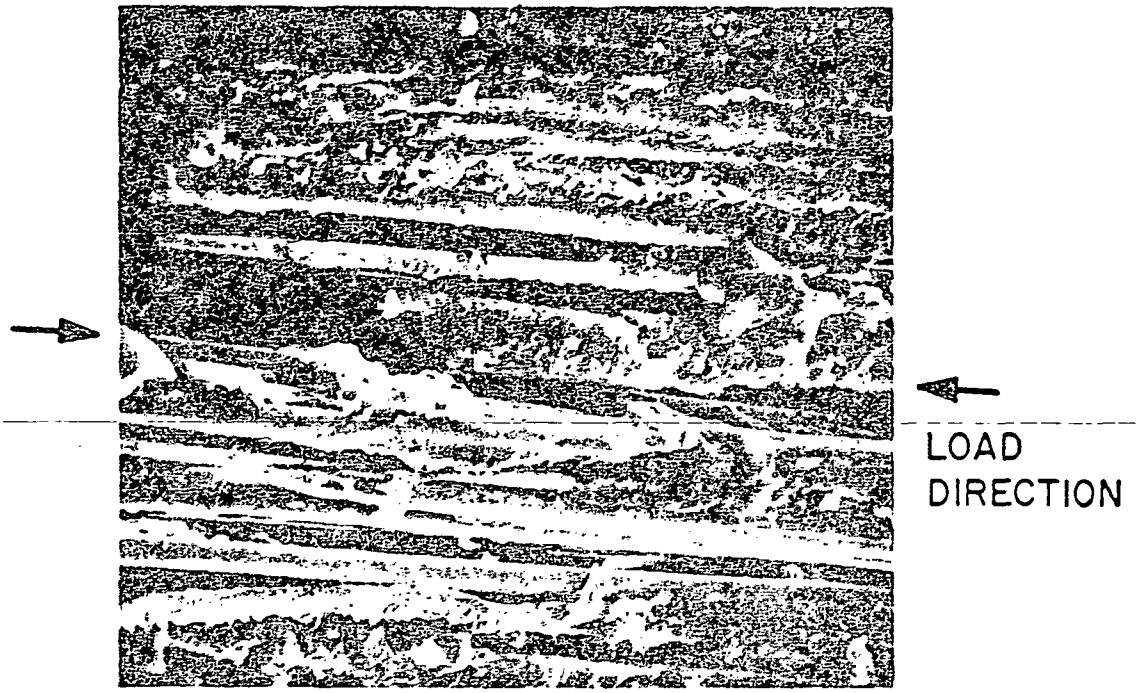

Figure (25a)-SEM Photomicrograph of the Failure Surface of E-Glass Sandwich Specimen No. 32, x 300

Figure (25b)-Magnified View of Figure (25a), x 1000

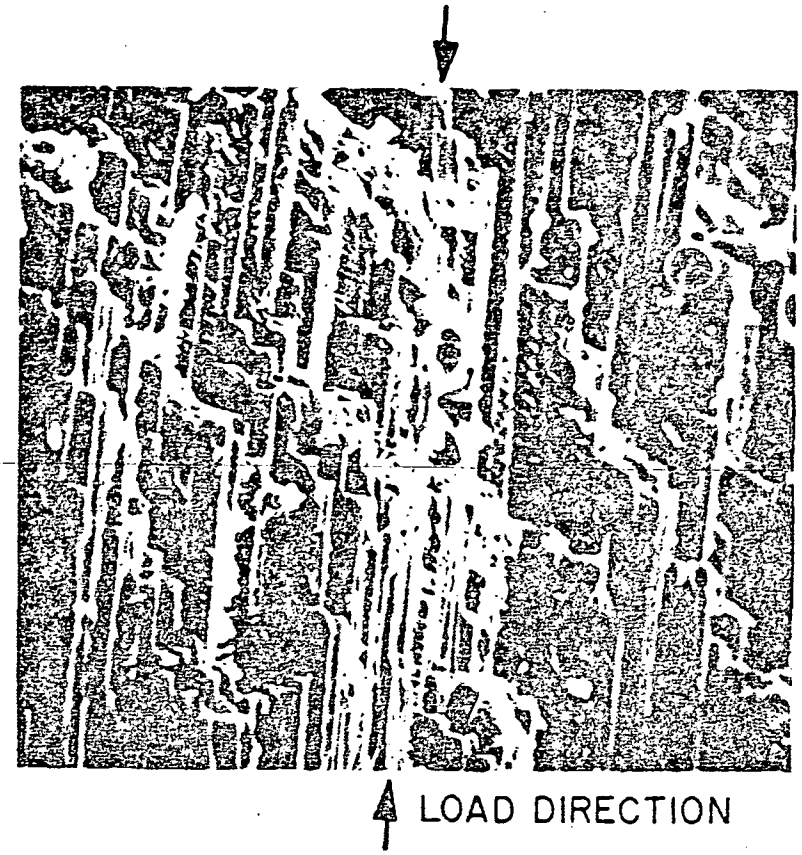

Figure (26a)-SEM Photomicrograph of the Failure Surface of HT-S Graphite Specimen No. 267, x 300

Figure (26b)-Magnified View of Figure (26a), x 3000

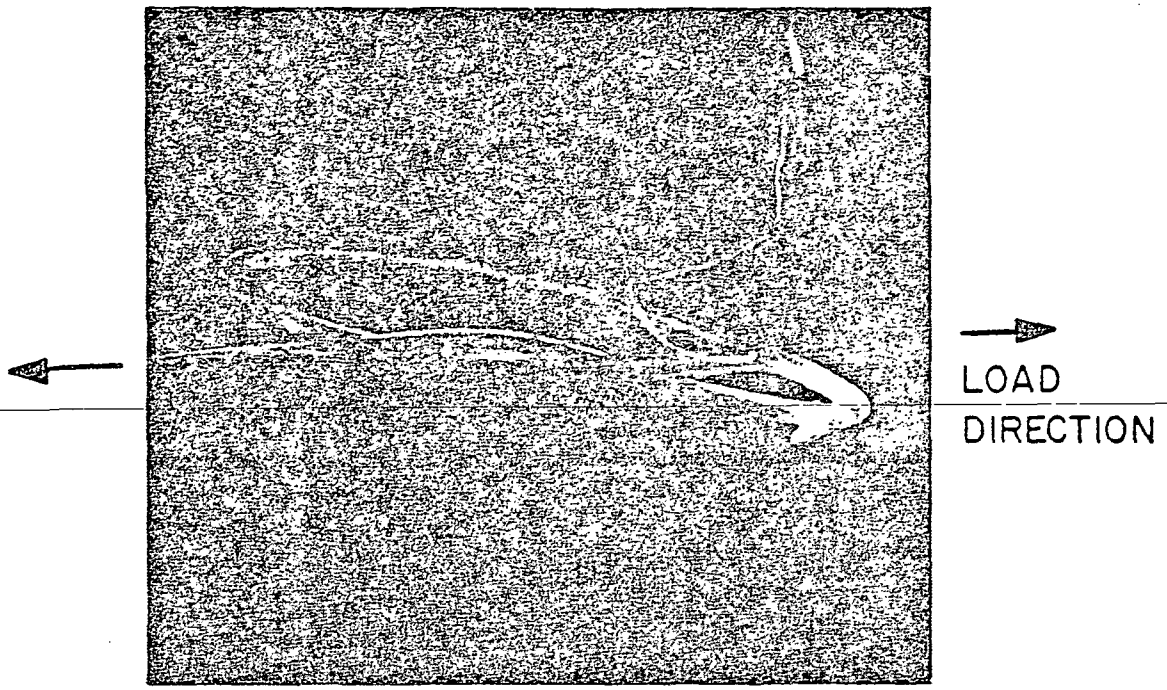

Figure (27a)-SEM Photomicrograph of a Knot of a Single PRD-49-III Fiber, x 200

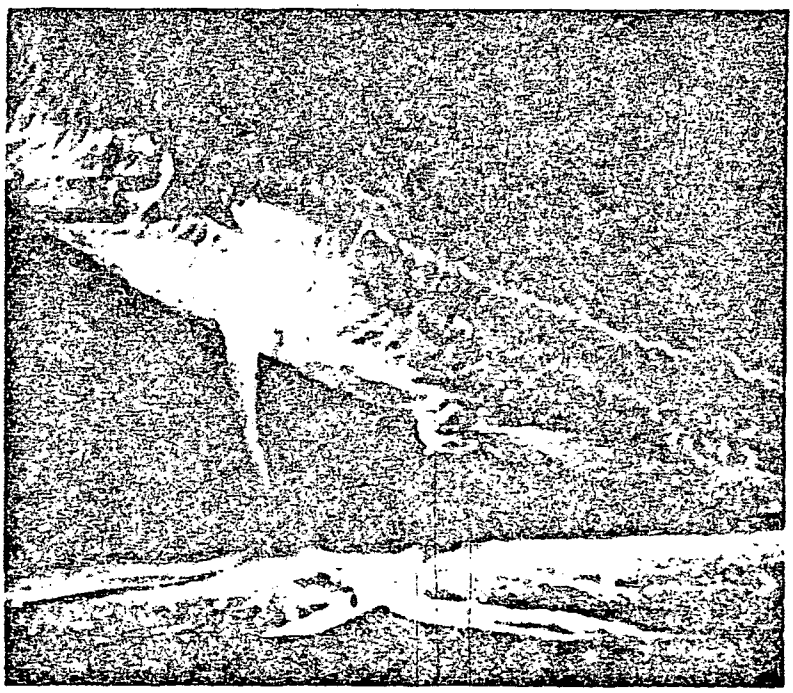

Figure (27b)-Magnified View of Figure (27a) Showing Appearance of Kink Bands on the Compression Side, x 2000

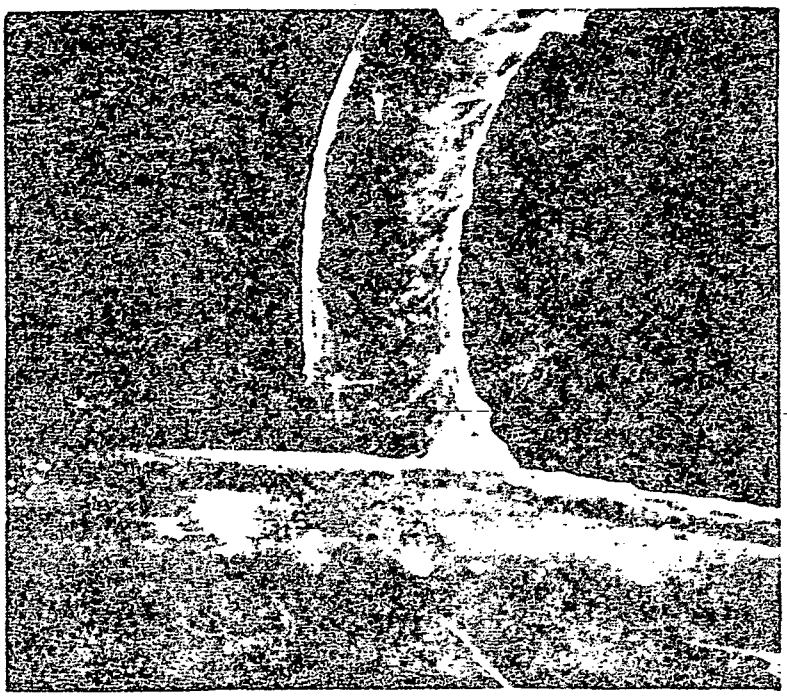

Figure (27c)-SEM Photomicrograph of the Knot for a Decrease in the Knot Radius, x 2000

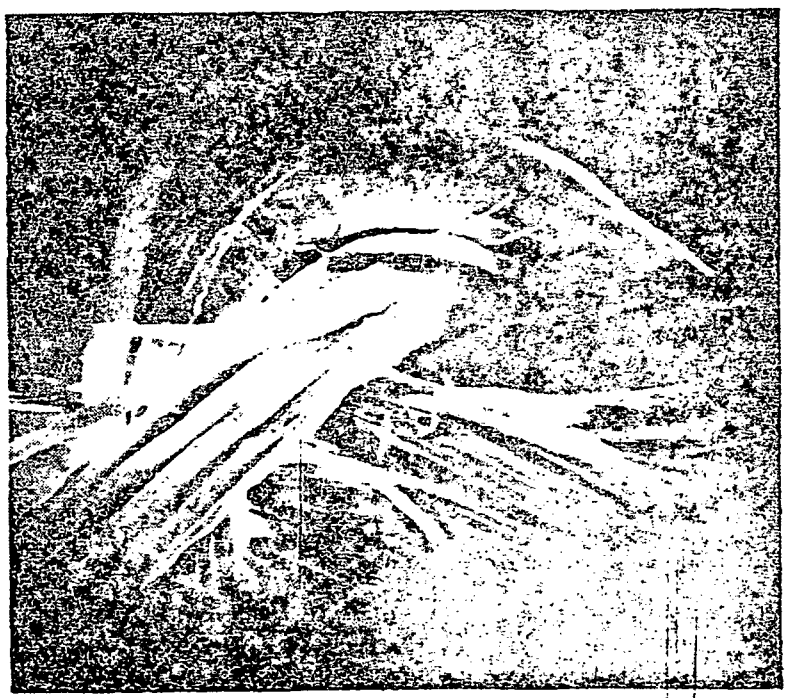

Figure (27d)-SEM Photomicrograph of a Two Fiber Knot Showing Complete Disintegration on the Tension Side and Slip Planes on the Compression Side, x 1500